

**BIOACTIVITY AND MECHANICAL BEHAVIOUR OF
NANOLAYER HYDROXYAPATITE COATING DEVELOPED
THROUGH SUPERPLASTIC EMBEDMENT OF
TITANIUM ALLOY**

SITI NUR BINTI HASAN

FACULTY OF ENGINEERING

UNIVERSITY OF MALAYA

KUALA LUMPUR

2013

BIOACTIVITY AND MECHANICAL BEHAVIOUR OF
NANOLAYER HYDROXYAPATITE COATING DEVELOPED
THROUGH SUPERPLASTIC EMBEDMENT OF
TITANIUM ALLOY

SITI NUR BINTI HASAN

DISSERTATION SUBMITTED IN FULFILLMENT OF
THE REQUIREMENTS FOR THE DEGREE OF
MASTER OF ENGINEERING SCIENCE

FACULTY OF ENGINEERING

UNIVERSITY OF MALAYA

KUALA LUMPUR

2013

UNIVERSITY OF MALAYA

ORIGINAL LITERARY WORK DECLARATION

Name of Candidate: SITI NUR BINTI HASAN

Matric No.: KGA100048

Name of Degree: MASTER OF ENGINEERING SCIENCE

Title of Dissertation (“this Work”):

BIOACTIVITY AND MECHANICAL BEHAVIOUR OF NANOLAYER
HYDROXYAPATITE COATING DEVELOPED THROUGH SUPERPLASTIC
EMBEDMENT OF TITANIUM ALLOY

Field of Study: ADVANCED MATERIALS

I do solemnly and sincerely declare that:

- (1) I am the sole author/write of this Work;
- (2) This Work is original;
- (3) Any use of any work in which copyright exists was done by way of fair dealing and for permitted purposes and any excerpt or extract from, of reference to or reproduction of any copyright work has been disclosed expressly and sufficiently and the title of the Work and its authorship have been acknowledged in this Work;
- (4) I do not have any actual knowledge nor ought I reasonably to know that the making of this work constitutes an infringement of any copyright work;
- (5) I hereby assign all and every rights in the copyright to this Work to the University of Malaya (“UM”), who henceforth shall be owner of the copyright in this work prohibited without the written consent of UM having been first had and obtained;
- (6) I am fully aware that if in the course of making this Work I have infringed any copyright whether intentionally or otherwise, I may be subject to legal action or any other action as may be determined by UM.

Candidate’s Signature

Date

Subscribed and solemnly declared before,

Witness’s Signature

Date

Name:

Designation:

ABSTRACT

The total joint replacement and mechanical stability are the vital components of the biomedical implant. In this study, Ti-6Al-4V is superplastically embedded with HA powder after being submitted to a heat treatment process to produce a new HA embedded layer with enhanced strength and good biocompatibility, which can be served as a good implant. Several properties of this new produced HA embedded layer has been analyzed from the perspective of bio-activity and scratch test. Numerous appropriate conclusions have been drawn. The results obtained, demonstrate that the HA embedded layer possesses good bioactivity properties and it is highly intact to the substrate, and that its stability is maintained even after immersion in simulated body fluid (SBF) for a period of 35 days.

University of Malaya

ABSTRAK

Kesempurnaan keseluruhan penyambungan dan kestabilan mekanik adalah dua komponen penting dalam implant biomedik. Dalam kajian ini, HA ditanam secara superplastik ke dalam Ti-6Al-4V yang telah menjalani rawatan haba dan proses ini menghasilkan lapisan HA yang baru yang telah ditingkatkan tahap kekuatannya dan kesesuaian biologinya dimana ia boleh digunakan sebagai implant yang berkualiti. Beberapa sifat lapisan HA telah dianalisa daripada sudut bioaktiviti dan ketahanannya terhadap goresan. Beberapa kesimpulan telah dibuat berdasarkan keputusan makmal dan analisisnya. Hasil yang diperolehi menunjukkan lapisan HA mempunyai sifat bioactivity yang baik dan ia melekat kuat dengan Ti-6Al-4V. Kestabilan lapisan HA masih kekal walaupun selepas 35 hari direndam dalam keadaan larutan badan (SBF).

ACKNOWLEDGEMENT

First and foremost I would like to express my utmost gratitude to Allah S.W.T for answering my prayers for giving me the knowledge, ability, strength and patience in completing this master's dissertation. This dissertation would not have been possible without the guidance and the help of several individuals who in one way or another contributed and extended their valuable assistance in my preparation and completion of this study.

I dedicate my special thanks to Dr. Iswadi bin Jauhari, my supervisor whose guidance, advice, help, support, sincerity and encouragement I will never forget. Dr. Iswadi has been my inspiration as I hurdle all the obstacles in the completion this research work. To the technical staff, Mr. Aziz, Mr. Nazarul Zaman and Mr. Zaini, thank you so much for their assistance in the technical part of this research work. They also have shared valuable insights in the relevance of my study.

Deepest dedication to my family especially my husband, Kamran Fakhar and my parents, Hasan bin Omar and Diwi binti Che Mat for their never ending love, care, prayer and support in whatever I do. Not forget my beloved siblings, thanks a lot for their love and support.

I would like to express appreciation to my friends for their support and encouragement. Thank you also to International Islamic University Malaysia (IIUM) and Ministry of Higher Education (MOHE) for sponsoring me in my study. Last but not least, my gratitude goes to UM for financing my research project under the Postgraduate Research Fund (Project No. PV053/2011A).

TABLE OF CONTENTS

ABSTRACT	ii
ABSTRAK	iii
ACKNOWLEDGEMENT	iv
TABLE OF CONTENTS	v
LIST OF FIGURES	viii
LIST OF TABLES	xi
LIST OF SYMBOLS AND ABBREVIATIONS	xii
CHAPTER 1: INTRODUCTION	
1.1 General	1
1.2 Research Objectives	3
1.3 Outline of Research	3
CHAPTER 2: LITERATURE REVIEW	
2.1 Superplasticity	5
2.1.1 Historical Background of Superplasticity	7
2.1.2 Characteristic of Superplastic Deformation	8
2.1.3 Mechanical Behaviour of Superplasticity	11
2.1.4 Superplasticity and Plasticity	12
2.1.5 Applications of Superplasticity	13
2.2 Titanium and Its Alloys	14
2.2.1 Classification of Titanium Alloys	16
2.2.1.1 α Alloys	16

2.2.1.2	$\alpha+\beta$ Alloys	17
2.2.1.3	β Alloys	18
2.2.2	Superplasticity of Titanium Alloys	19
2.2.3	Pre-heat Treatment of Ti-6Al-4V	22
2.3	Biomaterials	23
2.3.1	Hydroxyapatite	24
2.4	Production Methods of HA coating	25

**CHAPTER 3: MATERIALS PREPARATION AND
EXPERIMENTAL PROCEDURES**

3.1	Materials, samples, die and jigs preparation	27
3.1.1	Materials	27
3.1.2	Sample Preparation	29
3.1.3	Die and Jigs Preparation	29
3.2	Heat Treatment	31
3.3	Embedment Process	33
3.4	Bioactivity Test	35
3.5	Nanoscratch Test	37
3.6	Microhardness Test	39
3.7	Characterization Process	40
3.7.1	Field Emission Scanning Electron Microscope (FESEM)	41
3.7.2	Energy Dispersive X-ray (EDX) Analysis	44
3.7.3	X-Ray Diffraction (XRD)	45

CHAPTER 4: RESULTS AND DISCUSSIONS

4.1 Properties of the HA Embedded Layer and Its Characterizations	48
4.2 Biocompatibility of the HA Embedded Layer	52
4.3 Nanoscratch Properties of the HA Embedded Layer	59

CHAPTER 5: CONCLUSIONS AND RECOMMENDATIONS

5.1 Conclusions	71
5.2 Recommendations	72

REFERENCES	73
-------------------	-----------

University of Malaya

LIST OF FIGURES

Figure	Captions	Page
2.1	A dramatic demonstration of superplasticity in Cu-Al alloy (8000% elongation) (Hori et al., 1991)	5
2.2	Evolution of microstructure during superplastic deformation (Chandra, 2002)	6
2.3	Appearance of superplastic elongated specimens of ultra-fine grained materials at various test temperatures (Nakahigashi & Yoshimura, 2002)	7
2.4	Effect of grain size on strain rate (a) and superplastic deformation temperature (b) of Ti-6Al-4V, Ti-5Al-2.5Sn and Ti-6.5Al-3.3Mo-1.8Zr-0.26Si alloys (Bai et al., 2001; Combres and Blandin, 1995)	9
2.5	Cooperative GBS during superplastic deformation (Kaibyshev, 2002)	10
2.6	Female (a) and male (b,c) SPF processes (Demaid, 1992)	13
2.7	Phase Diagram of Ti-6Al-4V (Leyens and Peters, 2003)	16
3.1	Cutter	28
3.2	Dimension of the heat treated Ti-6Al-4V substrate before embedment	29
3.3	Design of die	30
3.4	Fabricated die	30
3.5	Design of jigs	31
3.6	Schematic diagram of the experimental set-up for heat treatment process	32
3.7	Heat treatment profile of Ti-6Al-4V	32
3.8	Front view illustration of Ti-6Al-4V and HA powder in the die	33

3.9	Fabricated die with the Ti-6Al-4V substrate and HA powder inside it, to be placed in the compression test machine for embedment process	34
3.10	Schematic diagram of experimental set-up in the compression machine	34
3.11	Superplastic embedment profile	35
3.12	Embedded sample immersed in the 20 ml SBF	36
3.13	Sample in SBF is placed in the furnace at constant temperature of 37 °C	36
3.14	Nanoscratch testing machine	38
3.15	Position of the sample and pendulum	38
3.16	Scratching illustration on the coating	39
3.17	Microhardness tester	40
3.18	FESEM principle	42
3.19	FESEM	42
3.20	Schematic diagram of EDX working system	44
3.21	XRD working system	46
3.22	XRD equipment	47
4.1	FESEM image of the (a) cross section (b) surface morphology at 8000 magnification and (c) surface morphology at 15000 magnification of an HA embedded layer	48
4.2	EDX spectrum on surface morphology of an HA embedded layer	50
4.3	Stress-strain relationship during embedment process	51
4.4	FESEM image of surface morphology of the HA layer after immersion in SBF for (a) 1 day, (b) 3 days, (c) 7 days, (d) 14 days, (e) 21 days, (f) 28 days and (g) 35 days	52
4.5	Thickness of the HA layer at different immersion time in SBF	56
4.6	XRD pattern of (a) pure HA powder and the HA layer after (b) 0 day (c) 1 day (d) 3 days (e) 7 days (f) 14 days (g) 21 days (h) 35 days of immersion in SBF	57

4.7	Hardness of the HA layer at different immersion time in SBF	58
4.8	FESEM image of 1000 μm length scratch track, scratched with 500 mN scratch load on a sample immersed for 7 days in SBF	59
4.9	FESEM images of the end of scratch track edge scratched at 50 mN load (15 k magnification)	60
4.10	FESEM images of the end of scratch track edge scratched at 100 mN load (15 k magnification)	62
4.11	FESEM images of the end of scratch track edge scratched at 300 mN load (15 k magnification)	64
4.12	FESEM images of the end of scratch track edge scratched at 500 mN load (15 k magnification)	66
4.13	EDX spectra of the end of scratch track edge, focusing on the (a) unpeeled-off and (b) peeled-off area of the HA layer of a sample immersed for 35 days in SBF	68

University of Malaya

LIST OF TABLES

Table	Captions	Page
2.1	Comparison between superplasticity and plasticity (Chandra, 2002)	12
2.2	Superplastic deformation conditions of selected titanium alloys and titanium matrix composites (Combres and Blandin, 1995; Frommeyer and Rommerskirchen, 1995; Hofmann et al., 1995; Imayev et al., 1999; Inagaki, 1995; 1996; Kim et al., 1999; Kobayashi et al., 1994; Kulikowski et al., 1995; Nieh et al., 1997; Ogawa et al., 1995; Salishchev et al., 2001; Tisler and Lederich, 1995)	20
3.1	Chemical composition of Ti-6Al-4V	27
4.1	Elemental percentage of EDX spectrum (Figure 4.2) on surface morphology of an HA embedded layer	51
4.2	Elemental percentage of EDX spectrum (Figure 4.13(a)) of the end of scratch track edge, focusing on the unpeeled-off area of the HA layer of sample immersed for 35 days in SBF	69
4.3	Elemental percentage of EDX spectrum (Figure 4.13(b)) of the end of scratch track edge, focusing on the peeled-off area of the HA layer of sample immersed for 35 days in SBF	69

LIST OF SYMBOLS AND ABBREVIATIONS

Symbols	Explanation
σ	Equivalent flow stress
K	Strength coefficient
$\dot{\epsilon}$	Equivalent strain rate
m	Strain-rate sensitivity

University of Malaya

Abbreviations	Explanation
HA	Hydroxyapatite
Ti	Titanium
SBF	Simulated body fluid
FESEM	Field Emission Scanning Electron Microscopy
EDX	Energy Dispersive X-ray
XRD	X-ray Diffractometer
FSS	Fine structure superplasticity
ISS	Internal stress superplasticity
GBS	Grain boundary sliding
SPD	Superplastic deformation
SPF	Superplastic forming
DB	Diffusion bonding
CaP	Calcium phosphate
TTCP	Tetra calcium phosphate
TCP	Tri calcium phosphate
SEM	Scanning Electron Microscopy
TEM	Transmission Electron Microscopy
Ca	Calcium
P	Phosphorus

CHAPTER 1

INTRODUCTION

1.1 General

Hydroxyapatite (HA) and titanium (Ti) are two prominent materials which are widely used in medical applications as implant materials (Ahmed and Jankowski, 2011; Caceres et al., 2008; Khalid et al., 2012; Parast et al., 2011; Saber-Samandari et al., 2011; Xuhui et al., 2009; Yildirim et al., 2005). Furthermore, the similarity of the chemical composition of HA to natural bone (Ahmed and Jankowski, 2011; Parast et al., 2011) and its ability to bond chemically to living bony tissue (Gu et al., 2003; Khalid et al., 2012) enhances its biocompatibility for biomedical implants. High corrosion and the excellent mechanical properties of Ti satisfy the load-bearing requirements of these implants. It also enables them to sustain large forces and assists them to retain their shapes after patient physical activity (Saber-Samandari et al., 2011). The HA coating can be deposited on a Ti alloy. However, several studies have raised concerns about its applicability on areas of high loading, such as the femoral and tibial cortical bones (Gu et al., 2003). Also, poor mechanical stability of the interface between coating and substrate may lead to complications either during a surgical operation or after implantation for a specified time (Collier et al., 1993; Cook et al., 1991; Nie et al., 2000; Simmons et al., 1999). The developed HA-based composites, through reinforcing HA with a mechanically superior secondary phase such as Ti (Dom et al., 2010), prove to be quite handy in enhancement of a weak HA layer. It has been shown that HA/Ti-6Al-4V coating can achieve better long-term

stability due to its superior mechanical properties, as compared to pure HA coating (Gu et al., 2003). Amongst several methods for obtaining HA/ Ti-6Al-4V coating, plasma spraying is one of the most commonly employed. However, it still has a number of limitations such as high cost (Yildirim et al., 2005) and poor adhesion of coating, which may result in its degradation from the substrate (Dom et al., 2010). Furthermore, the application of high temperature between 15273-30273 K in plasma spraying may lead to microstructural changes in substrate materials (Yildirim et al., 2005), as well as decomposition of HA (De Jonge et al., 2010).

The unique superplastic behaviour of materials has been widely recognized and consequently gained significant attention for several decades. It has been demonstrated that an HA-Ti layer with good bonding strength is successfully produced when the HA-Ti composite is implanted on superplastic Ti (Dom et al., 2010). Moreover, materials with such behaviour are able to exhibit a large degree of elongation prior to failure. However, the reduction rate in the thickness of the implanted layer after wear shows that the thicker layer is weaker than the thin layer (Parast et al., 2011). Also, a thin coating induces an osteogenic response in vitro (Yao et al., 2004), where bone regeneration and remodeling occur. Studies on the nanolayer coatings reveal that the nanolayer reflects the outstanding mechanical properties, e.g. higher hardness and better wear resistance (Khalid et al., 2012). Recently, nanolayer HA coating through superplastic embedment has been produced (Khalid et al., 2012). As a result, good adherent strength of the coating has been achieved. There are a few other factors, such as biocompatibility and mechanical properties of coating, which play a significant role in the success of the potential implants and hence warrant further studies (Cleries et al., 2000; Hench, 1998; Kokubo et al., 1990).

The previous studies (Parast et al., 2011; Khalid et al., 2012; Dom et al., 2010) which employed a superplasticity concept only focused on a wear test, but did not take into

account the bioactivity property. Therefore, the present research is concerned with a study of the bioactivity and mechanical properties of HA-embedded samples immersed in simulated body fluid (SBF) in order to define the coating's lifetime and its functionality as good joints. Bonding strength and stability between the HA layer and the substrate is evaluated upon resistance of the coating against scratch loads.

1.2 Research Objectives

The objectives of this research are:

1. To produce a bioactive HA embedded layer on Ti alloy with sufficient amount of HA elements through superplastic embedment.
2. To study the bioactivity of the HA embedded layer in SBF.
3. To study the mechanical properties between the HA embedded layer and the substrate.

1.3 Outline of Research

The research outlines are as follows:

1. Literature review

Understanding the theories and concepts related to HA, Ti-6Al-4V substrate, superplasticity, embedment method is completed by reviewing various journals, reference books, world wide website and previous dissertation report. Summary of the reviewed literatures is presented in Chapter 2.

2. Materials and experimental procedures

Explanation of the experimental works and properties of the embedded and substrate materials are presented in Chapter 3. The experimental works involve preparation of samples, die, puncher and jigs, heat treatment of Ti-6Al-4V, superplastic embedment process, bioactivity test, nanoscratch test and characterization process.

3. Characterization

Description of the characterization techniques is presented in Chapter 3. After embedment, Field Emission Scanning Electron Microscope (Zeiss FESEM) is used to characterize the surface morphology of the embedded layer and to determine layer thickness. Elemental composition of the layer is identified by Energy Dispersive X-ray (EDX) analysis. Details of the crystallographic structure of the layer are revealed by X-ray Diffraction (XRD, X Pert PRO) whilst surface hardness is measured by Vickers microhardness (Mitutoyo MK-17).

4. Results and discussion

Presentation and analysis of the results obtained are presented in Chapter 4, which contains the characterization of the HA embedded layer, its bioactivity and mechanical properties.

5. Conclusion and recommendations

Conclusion of the present research and recommendation for the further research activities are summarized in Chapter 5.

CHAPTER 2

LITERATURE REVIEW

2.1 Superplasticity

Superplasticity is the ability of a solid crystalline material to be deformed well beyond its usual breaking point during tensile loading, under a certain strain rate and temperature. Superplastic materials are found in metals (including aluminum, magnesium, iron, titanium and nickel-based alloys), ceramics (including monoliths and composites), intermetallics (including iron, nickel and titanium base) and laminates (Chandra, 2002). Previous study (Sieniawski and Motyka, 2007) reported that, two types of superplasticity are distinguished: fine structure superplasticity (FSS) - considered as an internal structural feature of material and internal stress superplasticity (ISS) - caused by special external conditions (e.g. thermal or pressure cycling) generating internal structural transformation that produce high internal stress dependent on external stress.

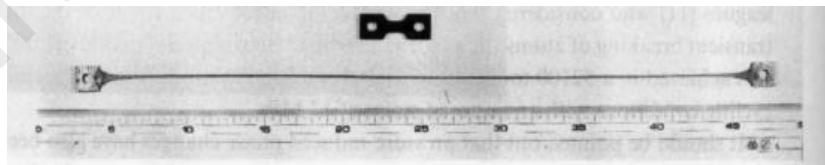


Figure 2.1: A dramatic demonstration of superplasticity in Cu-Al alloy (8000% elongation
(Hori et al., 1991)

Superplastically deformed material gets thinner in a very uniform manner, rather than forming a "neck" (a local narrowing) which leads to fracture (Dieter, 1986). The

current world record for elongation in metal stands at 8000% elongation in commercial bronze by Hori et al., 1999 is shown in Figure 2.1. Superplasticity represents an inelastic behavior with high strain rate sensitivity, grain switching and grain boundary sliding (GBS) (Chandra, 2002; Hiraga et al., 2010; Langdon, 1994). In superplastic material, grains remain nearly equiaxed even after deformation so it can be concluded that the primary mechanism in superplasticity is grain boundary sliding (Chandra, 2002; Vetrano, 2001). As shown in Figure 2.2, in superplasticity the grains change their neighbors and the original structure is restored. Through grain boundary sliding, the inelastic strain is produced (Chandra, 2002).

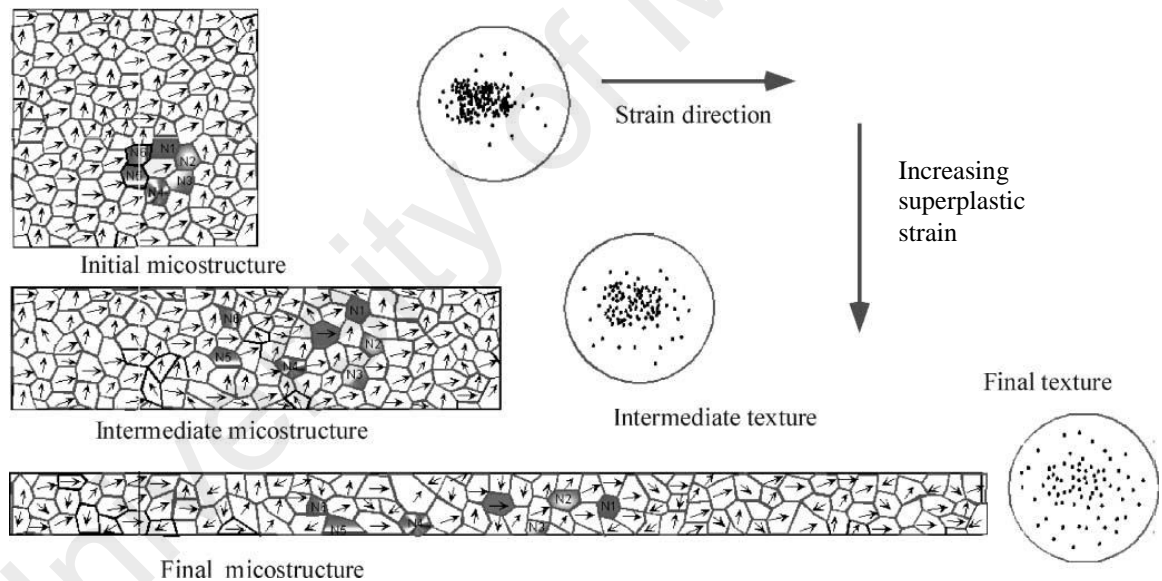


Figure 2.2: Evolution of microstructure during superplastic deformation (Chandra, 2002)

The appearance of the superplastic elongated specimens of the ultra-fine grained materials at various test temperatures is presented in Figure 2.3. The ultra-fine grained materials exhibit superplastic elongation of over 1000%. Elongation increases with the increase in test temperature.

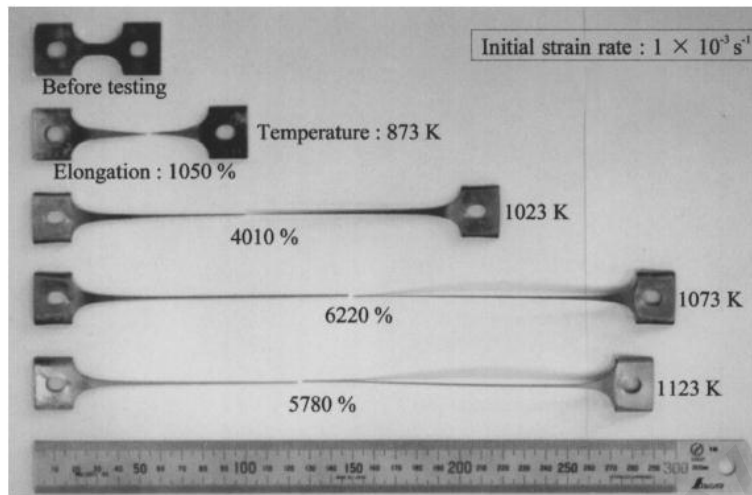


Figure 2.3: Appearance of superplastic elongated specimens of ultra-fine grained materials at various test temperatures (Nakahigashi & Yoshimura, 2002)

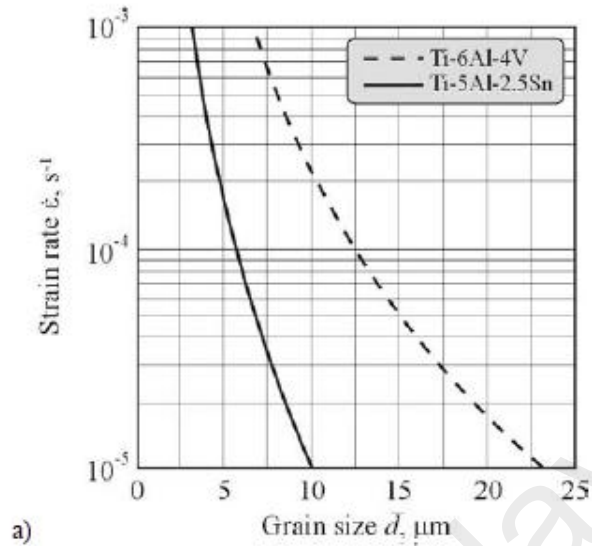
2.1.1 Historical Background of Superplasticity

Rosenhain, Houghton and Bingham are the people who first reported the phenomena of superplasticity on a eutectic alloy of Zn-Al-Cu in 1920. In 1934, Pearson did the earliest amazing observations on Bi-Sn eutectic alloy with a tensile elongation of 1950% without failure (Langdon, 2009). He also showed that the size and the shape of the grains of the superplastic alloys did not change during the deformation. After that, lots of research activities had been carried out on superplasticity (Hori et al., 1991; Nieh et al., 1997; Hamilton et al., 1988).

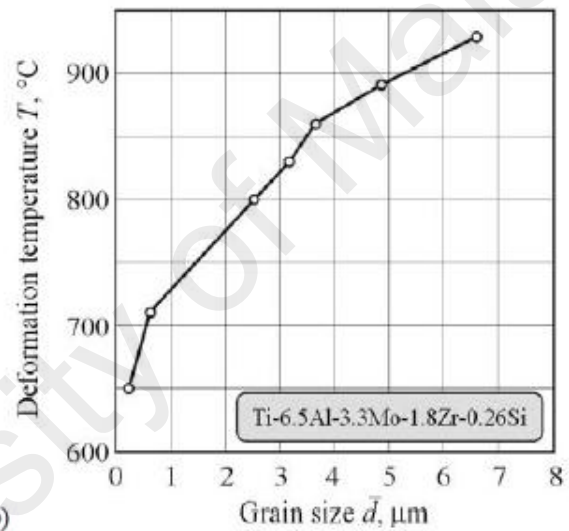
2.1.2 Characteristic of Superplastic Deformation

There are three primary requirements to influence materials properties for the success of superplasticity of an alloy which are: (1) a fine and stable grain size (usually less than 10 μm), (2) processing temperature at or above 0.4 of the melting temperature (measured in K), and (3) a suitable strain rate (dependent upon the properties of the specific alloy, strain rate at which superplasticity is optimized generally falls between 10^{-4} and 10^{-2} sec^{-1} for most materials and processing combinations) (Elias et al., 2007).

Main criterion of superplastic materials is the possibility of obtaining fine-grained and equiaxial microstructure which assures the occurrence of maximum deformation. Grain refinement is essential to obtain enhanced superplasticity at lower temperatures or high strain rates. It was established that grain refinement causes increase of strain rate and decrease of superplastic deformation temperature as shown in Figure 2.4 (Bai et al., 2001; Combres and Blandin, 1995). Number of grain boundaries increases by the grain refinement which helps the grain boundary sliding to occur at lower temperature with high strain rate. Forming rate must be sufficiently high to satisfy the current fabrication speed (Higashi and Mabuchi, 1997) and lower forming temperature would save the fabrication energy (Pu et al., 1995).



a)



b)

Figure 2.4: Effect of grain size on strain rate (a) and superplastic deformation temperature (b) of Ti-6Al-4V, Ti-5Al-2.5Sn and Ti-6.5Al-3.3Mo-1.8Zr-0.26Si alloys (Bai et al., 2001; Combres and Blandin, 1995)

Equiaxed microstructure favours proceeding of GBS in the mechanism of superplastic deformation which is controlled by GBS (Hsiao and Huang; 2002) and possesses a strong grain size dependency (Sherby and Wadworth; 1984). Fine grained polycrystalline materials with grains elongated crosswise deformation direction GBS is limited. Recent

experiments on microstructural processes occurring during superplastic deformation (Kaibyshev, 2002; Mukherjee, 2002; Nieh et al., 1997) proved the existence of cooperative grain-boundary sliding related to sliding of groups of grains (Figure 2.5). It was found that operation of that mechanism does not depend on crystal lattice type and dislocation activity in grains. Occurrence of cooperative GBS is conditioned mainly by structure of grain boundaries in polycrystal. It was determined that cooperative GBS is also connected with rotation and migration of whole grain assemblies.

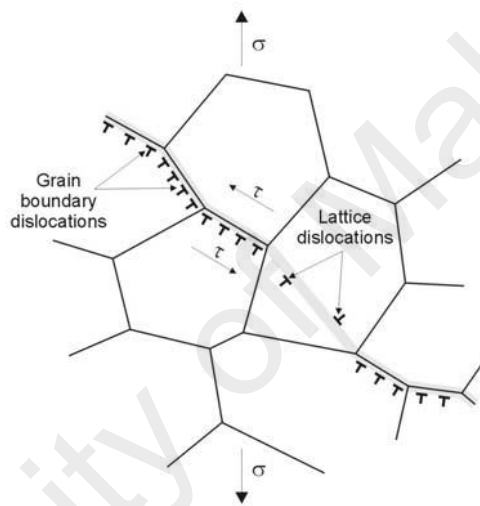


Figure 2.5: Cooperative GBS during superplastic deformation (Kaibyshev, 2002)

Superplasticity which can be considered as the movement of matter is a temperature dependence mechanism and is commonly occurs at elevated temperature in most materials. The deformation temperature for superplasticity should be about 0.4 of the melting temperature (K); for titanium alloys this is about 90% of the beta-transus temperature. Plastic deformation at these high temperatures is primarily due to the permanent deformation under current stress called creep. For favor creep deformation, two metallurgical properties are required: (1) extremely fine microstructures, because creep is

primarily controlled by grain boundary sliding and (2) stability of the fine structures at the high deformation temperatures (Leyens and Peters, 2003).

High strain-rate sensitivity, m (typically close to 0.5) is one important factor in superplastic deformation which stabilizes against localized necking and results in high plastic elongation (Chandra, 2002; Vetrano, 2001). Different materials demonstrate different sensitivity on the strain rate and it depends on the structure of the material.

2.1.3 Mechanical Behaviour of Superplasticity

Superplastic models are typically written as:

$$\sigma = K\dot{\epsilon}^m \quad (2.1)$$

where σ is the equivalent flow stress, K is the strength coefficient, $\dot{\epsilon}$ is the equivalent strain rate and the slope is $\partial(\ln \sigma)/\partial(\ln \dot{\epsilon})$ which represents the strain-rate sensitivity parameter. In superplastic deformation (SPD) process, higher the value of m , the higher is the superplastic properties (large elongation). It can be theoretically shown that m represents the resistance to necking and provides more diffused necking during deformation, prolonging the stretching process (Chandra, 2002)

2.1.4 Superplasticity and Plasticity

In order to develop a basic understanding of the superplastic behavior of materials, it is worthwhile to compare superplasticity with other inelastic processes, especially elastic-plastic and elevated temperature creep processes. Table 2.1 outlines some of the basic differences between plastic and superplastic behavior.

Table 2.1: Comparison between superplasticity and plasticity (Chandra, 2002)

Superplasticity	Plasticity
Superplasticity represents an inelastic behavior with high strain rate sensitivity	Plasticity represents inelastic behavior with no rate dependence
The effect of strain hardening is secondary	Flow stress primarily increased due to strain hardening
Grain switching, GBS are the primary mechanisms	Grain neighbours remain as such at all times
Texture decreases (grain orientation becomes random increasing with strain)	Texture decreases (preferred orientation in the principle plastic strain direction)
Deformation primarily due to GBS with diffusion and dislocation as the accommodating mechanisms	Deformation primarily due to dislocational activities
Deformation reduces the initial anisotropy	Deformation induces a strong anisotropy
Failure due to cavity initiation, growth and finally by geometric instability	Failure due to material and geometric instability

2.1.5 Applications of superplasticity

Superplasticity is used to form parts in the automotive, aerospace and many other smaller industries. Application of superplastic deformation in industrial forming of alloys offers advantages related mainly to possibility of producing elements having complex shape using one technological operation under low unit pressure (Demaid, 1992). Generally superplastic forming (SPF) process is carried out under pressure in protective atmosphere and two main methods are distinguished: female forming (Figure 2.6 (a)), and male forming (Figure 2.6 (b, c)).

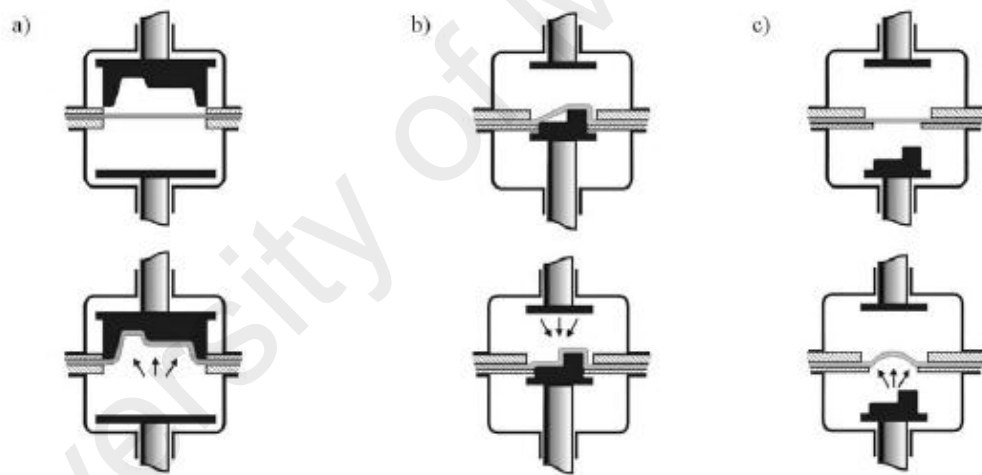


Figure 2.6: Female (a) and male (b,c) SPF processes (Demaid, 1992)

It should be emphasized that relatively low tool wear occurs resulting from low unit pressure and small slide between sheet and die. In some cases, when maximum pressure leads to local necking of product walls, initial bubble-blowing is used (Figure 2.6 (c)) (Demaid, 1992). Advantages of SPF can be assessed on producing of aircraft components. Emergency door for BAe 125 airplane produced from aluminium alloy using conventional methods is composed of 80 detail pressings and about 1000 fasteners. Fabrication of the

same product from titanium alloy using SPF enables reduction of the large parts number to 4 and fasteners number to 90. It gives a cost saving of 30% overall (Demaid, 1992). Application of SPF and diffusion bonding (SPF/DB) for producing aft fuselage of F-15E fighter allowed to eliminate 726 parts and about 10,000 fasteners (Martin and Evans, 2000).

Superplastic forming of aluminium sheet components with complex shapes is attractive for a wide variety of applications in the aerospace, automotive and medical device industries. It is capable to reduce the amount of material loss and time required for machining components from thick plates in aerospace and transport industries. In advanced aerospace applications, 70 to 90% of the material purchased is machined away in order to create the complex geometry which satisfies the mechanical requirement with the minimum possible component weight. Superplastic forming enables redesigned components to be fabricated with little or no loss of material to machining. Numerous demonstration components have been fabricated for aerospace and automotive applications. Few latest studies in this regards are (Liu et al., 2010; Narayan et al., 2010; Xinghao et al., 2007)

2.2 Titanium and Its Alloys.

Last decades, Ti alloys have been widely used in the aeronautical industry and for biomedical applications. The interest in Ti and its alloys can be explained by its remarkable properties, such as a high tenacity, a good heat resistance, a particular resistance to corrosion, biocompatibility with no adverse tissue reaction, its superplastic capacities and last but not least its interesting specific mass when compared to other high strength alloys such as steels (Azevedo and Santos, 2003; Fonseca et al., 2003; Long and Rack, 1998; Wang, 1996)

Specifically, for biomedical applications, Ti and its alloys are widely used because of their desirable properties, such as good relatively low modulus, good fatigue strength and corrosion resistance (Niespodziana et al., 2006). The low elastic modulus of Ti and its alloys is generally viewed as a biomechanical advantage because the smaller elastic modulus can result in smaller stress shielding. Low densities of titanium alloys give high specific strength-to-weight ratios allowing lighter and stronger structures. However, Ti and its alloys have relatively poor tribological properties because of its low hardness (Liu et al., 2004).

Depending on the predominant phase or phases in their microstructure and alloying additions, Ti alloys are categorized into three main categories:

1. Alpha (α) alloys - contain neutral alloying elements (such as tin) and/ or α stabilisers (such as aluminium or oxygen) only. These are not heat treatable.
2. Alpha-beta ($\alpha + \beta$) alloys - which are metastable and generally include some combination of both α and β stabilizers, and which can be heat treated.
3. Beta (β) alloys - which are metastable and which contain sufficient β stabilizers (such as molybdenum, silicon and vanadium) to allow them to maintain the β phase when quenched, and which can also be solution treated and aged to improve strength.

Figure 2.7 shows the phase diagram of Ti-6Al-4V. Above β -transus temperature the single β phase field is separated from two-phase $\alpha + \beta$ field and the whole microstructure is composed of β grain (Leyens and Peters, 2003; Polmear, 1981). At the temperature of below the transus temperature α nucleates at grain boundaries and grows into the β grain. The existence of vanadium causes to enrich β phase and stabilizes this phase at lower temperatures (Leyens and Peters, 2003). At room temperature, the microstructure is mainly

composed of hexagonal close-packed structure α phase and a little of body-centre cubic β phase (Polmear, 1981).

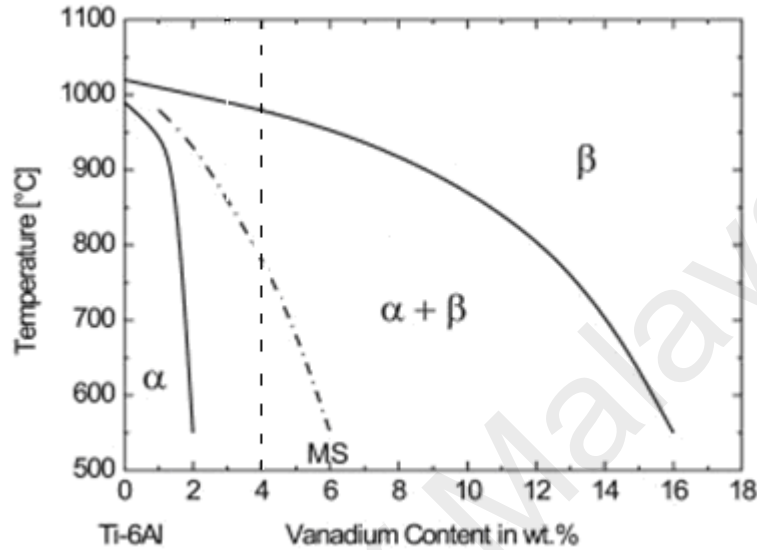


Figure 2.7: Phase Diagram of Ti-6Al-4V (Leyens and Peters, 2003)

2.2.1 Classification of Titanium Alloys

2.2.1.1 α Alloys

The single-phase and near-single-phase α alloys of Ti are non-heat treatable and have good weldability. The generally high aluminium content of this group of alloys ensured good strength characteristics and oxidation resistance at elevated temperatures (in the range of 600 to 1100 °F). α alloy has low to medium strength (Leyen and Peters, 2003) but it cannot be heat treated to develop higher mechanical properties because they are single-phase alloys. α alloys possess the highest corrosion resistance. More highly alloyed near- α alloys offer optimum high temperature creep strength and oxidation resistance. α

alloys also present good notch toughness, reasonably good ductility and excellent mechanical properties at cryogenic temperatures. α alloys are primarily used in the chemical and process engineering industries (Leyen and Peters, 2003).

2.2.1.2 α - β Alloys

The addition of controlled amounts of β -stabilizing alloying elements causes β phase to persist below β transus temperature, down to room temperature, resulting in two-phase system. These two-phase Ti alloys can be strengthened significantly by heat treatment consisting of a quench from some temperature in the α - β range, followed by an aging cycle at a somewhat lower temperature. β -phase transformation which would normally occur on slow cooling is suppressed by the quenching. The aging cycle causes the precipitation of some fine α particles from the metastable β , imparting a structure that is stronger than the annealed α - β structure. Although heat-treated α - β alloys are stronger than the α alloys, their ductility is proportionally lower. α - β alloys are heat treatable and most are weldable. Typical properties include:

1. Strength levels are medium to high
2. High temperature creep strength is not as good as most α alloys
3. Cold forming may be limited but hot forming qualities are normally good
4. Many alloys can be superplastically formed

The most commonly used α - β alloy is Ti-6Al-4V (Joshi, 2006), developed in many variations of the basic formulation for the widest possible choice of key properties and for many widely differing applications.

2.2.1.3 β Alloys

The high percentage of β -stabilizing elements in these alloys results in a microstructure that is substantially β . The high amount of added beta-stabilizer elements decreases the temperature of the allotropic transformation (α - β transition) of Ti (Froes and Bomberger, 1985). The metastable β can be strengthened considerably by heat treatment (Karasevskaya et al., 2003). β alloys are very brittle at cryogenic temperatures and are not meant to be applied at high temperatures, as they show low creep resistance. β alloys are used in highly specialized burn-resistance and corrosion resistance applications due to their high densities and poor ductility (Joshi, 2006). β or near β alloys are:

1. Fully heat treatable
2. Generally weldable
3. Capable of high strengths
4. Possess good creep resistance up to intermediate temperatures
5. Excellent formability can be expected in the β alloys in the solution treated condition

β -type alloys have good combinations of properties in sheet, as fasteners and are ideal for spring applications. Some alloys offer uniform property levels through heavy sections. The higher alloy content of β alloys increases the density of β alloys typically by 7-10% compared to Ti-6Al-4V. Typical β alloys include Ti3Al8V6Cr4Mo4Zr ASTM Grade 19, Ti15Mo3Nb3Al2Si ASTM Grade 21, Ti10V2Fe3Al AMS 4983, 4984, 4987 and Ti15V3Cr3Sn3Al AMS 4914. It is only the metastable β alloys which are heat treatable by solution treatment and ageing. Fully stable β alloys can only be annealed.

2.2.2 Superplasticity of Titanium Alloy

One of the Ti alloys which has been extensively studied in aspect of superplasticity is widely used Ti-6Al-4V alloy. Results concerning research on this alloy published in world scientific literature indicate meaningful progress in evaluation and applications of superplasticity in last 30 years. In the beginning of 70's maximum superplastic tensile elongation of Ti-6Al-4V alloy was about 1000% at the strain rate of 10^{-4} s^{-1} (Grabski, 1973), whereas in few last years, special thermomechanical methods were developed enabling doubling of tensile elongation and increase the strain rate 100 times (Chandra, 2002) (Table 2.1). Relatively new group of superplastic Ti alloys are TiAl or Ti₃Al intermetallics based alloys (Table 2.2). It is well known that intermetallics based alloys have a high relative strength, and good high-temperature creep resistance. Widespread usage of those materials is limited mainly by their low plasticity precluding forming of structural components using conventional plastic working methods. In this case pursuit to obtain fine-grained microstructure enabling superplastic deformation seems to be very promising (Hofmann et al., 1995; Imayev et al., 1999; Kobayashi et al., 1994; Nieh et al., 1997).

Table 2.2: Superplastic deformation conditions of selected Ti alloys and Ti matrix composites (Combres and Blandin, 1995; Frommeyer and Rommerskirchen, 1995; Hofmann et al., 1995; Imayev et al., 1999; Inagaki, 1995; 1996; Kim et al., 1999; Kobayashi et al., 1994; Kulikowski et al., 1995; Nieh et al., 1997; Ogawa et al., 1995; Salishchev et al., 2001; Tisler and Lederich, 1995)

Alloy	Phase composition	Elongation (%)	Grain size (μm)	Temperature ($^{\circ}\text{C}$)	Strain rate (s^{-1})
Two-phase $\alpha+\beta$ alloys					
Ti-4Al-4Mo-2Sn-0.5Si (<i>IMI550</i>)	$\alpha+\beta$	2000	4	885	5×10^{-4}
Ti-4.5Al-3V-2Mo-2Fe (<i>SP-700</i>)	$\alpha+\beta$	2500	2÷3	750	10^{-3}
Ti-5Al-2Sn-4Zr-4Mo-2Cr-1Fe (β - <i>CEZ</i>)	$\alpha+\beta$	1100	2÷3	72	2×10^{-4}
Ti-6Al-4V	$\alpha+\beta$	2100	2	850	10^{-2}
Ti-6Al-2Sn-4Zr-2Mo	$\alpha+\beta$	2700	1÷2	900	10^{-2}
Ti-6Al-2Sn-4Zr-6Mo	$\alpha+\beta$	2200	1÷2	750	10^{-2}
Ti-6Al-7Nb (<i>IMI367</i>)	$\alpha+\beta$	300	6	900	3×10^{-4}
Ti-6.5Al-3.7Mo-1.5Zr	$\alpha+\beta$	640	6÷7	600	10^{-4}
Ti-6Al-2Sn-2Zr-2Mo-2Cr-0.15Si	$\alpha+\beta$	2000	4	885	5×10^{-4}
Intermetallics based alloys					
Ti-24Al-11Nb	$\alpha_2(\text{Ti}_3\text{Al}) + \beta$	1280	4	970	10^{-3}
Ti-46Al-1Cr-0.2Si	$\gamma(\text{TiAl}) + \alpha_2(\text{Ti}_3\text{Al})$	380	2÷5	1050	10^{-3}
Ti-48Al-2Nb-2Cr	$\gamma(\text{TiAl}) + \alpha_2(\text{Ti}_3\text{Al})$	350	0, 3	800	8.3×10^{-4}
Ti-50Al	$\gamma(\text{TiAl}) + \alpha_2(\text{Ti}_3\text{Al})$	250	<5	900-1050	$2\times 10^{-4} \div 8.3\times 10^{-3}$
Ti-10Co-4Al	$\alpha+\text{Ti}_2\text{Co}$	1000	0.5	700	5×10^{-2}

Titanium matrix composites					
Ti-6Al-4V + 10% TiC	α +TiC	270	5	870	1.7×10^{-4}
Ti-6Al-4V + 10% TiN	α +TiN	410	5	920	1.7×10^{-4}

Ti alloy has the similar tension characteristics as materials that have a plastic deformation above 200% and a grain size of less than 10 μm . Typically, Ti alloys do not exhibit fine-grain superplasticity in the beta phase field due to rapid grain growth. In this technology, superplasticity can be achieved by an addition of one compound. The new alloy restricts the beta growth and stabilizes a fine, equiaxed beta grain size at the deformation temperature, thereby enabling superplasticity. The new strain rates are of a magnitude of 2 – 3 times higher when compared to conventional superplasticity.

The technology of superplasticity may be highly beneficial in various types of manufacturing industries, such as aerospace, aviation, transportation, and other industries that involve metalworking and lightweight materials. The demand in strong, lightweight materials that have superplasticity characteristics, are expected to grow at a higher rate than the general market. The Ti based alloy has several benefits over existing technologies:

1. Ability to form intricate shapes not possible by other approaches or techniques.
2. Higher production rates than conventional superplasticity materials.
3. Lower manufacturing and equipment costs to produce materials of the same technical specifications.
4. Ability to form near-net/net shapes with enhanced mechanical properties on smaller capacity presses.
5. Improved chemical homogeneity due to enhanced diffusion rates.
6. Reduced processing and production costs and improved performance with strength, stiffness and microstructure.

2.2.3 Pre-heat Treatment of Ti-6Al-4V

Pre-heat treatment is an important process prior to superplastic embedment. Ti and Ti alloys are heat treated in order to:

1. Reduce residual stresses developed during fabrication (stress relieving) or techniques.
2. Produce an optimum combination of ductility, machinability, and dimensional and structural stability (annealing).
3. Increase strength (solution treating and aging)
4. Optimize special properties such as fracture toughness, fatigue strength, and high-temperature creep strength.

Rapid cooling above the beta transus is the best pre-heat treatment for superplastic deformation of Ti-6Al-4V. According to the phase diagram of Ti-6Al-4V in Figure 2.7, fully beta-phase structure is achieved by heating the Ti-6Al-4V above the beta transus temperature. The presence of beta-phase can strongly improve the superplasticity of Ti alloys. As reported by Malakarjun et al., (2003), formability of beta-phase is higher than alpha-phase at superplastic temperature and the existence of beta-phase reduces the optimum superplastic temperature. Rapid cooling from the above beta transus produces a structure consisting of all alpha' (Ti martensite) (Polmear, 1981) which consists of parallel-sided plates or lath with high dislocation density and high internal stresses due to the rapid transformation (Smith, 1993).

2.3 Biomaterials

A biomaterial is a synthetic material used to replace part of a living system or to function in intimate contact with living tissue (Shi, 2004). Biomaterials interact with biological systems without causing any unacceptable harm to the body (Latka et al., 2010). Biomaterials can be derived either from nature or synthesized in the laboratory using a variety of chemical approaches utilizing metallic components or ceramics. They are often used and/or adapted for a medical application, and thus comprise whole or part of a living structure or biomedical device which performs, augments, or replaces a natural function. Such functions may be benign, like being used for a heart valve, or may be bioactive with a more interactive functionality such as HA coated hip implants. Biomaterials are also used every day in dental applications, surgery, and drug delivery. A biomaterial may also be an autograft, allograft or xenograft used as a transplant material.

To be used as an implant, biomaterials must exhibit high biocompatibility and long life in the human body (more than 20 years) without any corrosion, fracture or delaminating (Conforto et al., 2004; Javed and Romanos, 2010). Good mechanical properties are required, mostly high resistance to fatigue and wear. Good mechanical interlocking is also necessary because the fixation of the implant is not guaranteed by the chemical interactions with the biological tissue which are too weak. A growing interest has been observed in the field of development of new biomaterials which present biocompatibility associated with high wear resistance and low wettability (Barbieri et al., 2002). Designing the new materials, from well-known old one, by an adequate surface treatment process has been one of the trends of materials research subjects (Czarnowska et al., 1999).

2.3.1 Hydroxyapatite

HA is a well-established bioactive ceramic material capable of forming strong chemical bonds with natural bones (Xuhui et al., 2009). As a highly biocompatible material, it quickly improves bone-biomaterial interface, conferring, therefore on the prostheses good osteointegration capabilities (Yildirim et al., 2005). HA has been used since 1990 as coating on the prostheses of e.g. hips, knees and teeth in order to enhance their biointegration to a bone (Tattner et al., 2004) due to its similar chemical composition to natural bone (Ahmed and Jankowski, 2011). Orthopedic and dental implants are mostly bio-inert metal alloys and do not offer a good chemical bond to bone as HA does (Chai and Ben-Nissan, 1999). Also, porous HA coatings are known to promote bone regeneration (Wei et al., 1999). One major application of HA is to serve as a cover material for Ti or other metals used in implants (Suchanek and Yoshimura, 1998). In this case, the biocompatibility of the implant is assured by HA, while the mechanical properties are provided by metal substrate (Gu et al., 2003). HA coated Ti alloy implants combine the bioactivity of HA and the mechanical properties of titanium alloy. Zhang et al. (2006) stated that HA coating can protect the Ti alloy substrates against corrosion in the biological environment, and also can be as a barrier against the release of toxic metal ions from the substrates into the living body.

2.4 Production Methods of Hydroxyapatite Coating

For several decades now, coating technology has found a wide array of applications. These include functional coating, decorative coating, industrial coating, thermal barrier coating, biomaterial coating and others. Whatever the application is, the mechanical properties of the deposited coatings should be sufficient to satisfy the application's requirements.

There are several methods existed for coating HA on a Ti alloy substrate (Meng et al., 2008; Hsieh et al., 2002; Ding, 2003; Narayanan et al., 2006). Various methods are available for production of HA coatings, which include sol-gel (Liu et al., 2002; Hsieh et al., 2002), sputtering (Ktessabi and Hamdi, 2002; Hamdi and Ktessabi, 2001), pulsed laser deposition (Wang et al., 1997), and thermal spraying (Kweh et al., 2000; MacDonald et al., 2001; Lynn and DuQuesnay, 2002). Among them, plasma spraying is the most popular method due to its feasibility and good coating mechanical properties (Ding et al., 2001). However, the high cost and also, extremely high temperatures such as between 15000-30000 °C are underestimated that cause microstructural changes in the substrate implant material (Yildirim et al., 2005) and also degradation of HA particles into other less stable phases of calcium phosphate (CaP) including tetra calcium phosphate (TTCP), tri calcium phosphate (TCP) and amorphous CaP (Radin and Ducheyne, 1992). In addition, it is difficult to prepare a uniform coating on metal implant with a complex shape via plasma spraying (Dom et al., 2010). Also, the coating has a tendency to degrade from the Ti substrate due to low bonding strength (Jansen et al., 1991) which is a critical factor in long-term stability of the implant material (Liu et al., 2005).

Embedment is a material engineering process by which ions or elements of a material can be implanted into another solid and it can change the physical properties of the solid. A mutual reaction occurs between granules and alloy and it seems that there is a chemical reaction in the interface of the granules and Ti alloy in the embedment process (Nonami et al, 1998).

University of Malaya

CHAPTER 3

MATERIALS PREPARATION AND EXPERIMENTAL PROCEDURES

3.1 Materials, Samples, Die and Jigs Preparation

3.1.1 Materials

The substrate material used in this research is Ti alloy Grade 5, Ti-6Al-4V. The Grade 5 Ti alloy is heat treatable and is alloyed with 6% aluminum and 4% vanadium, by weight. The chemical composition of this alloy is listed in Table 3.1. Ti-6Al-4V is classed as an alpha-beta alloys, which is metastable and generally include some combination of both alpha and beta stabilizers, and which can be heat treated. Ti-6Al-4V is the most widely used Ti alloy with the excellent combination of strength, corrosion resistance, weld and fabricability. Consequently, Ti-6Al-4V has been used in various applications and one of them is medical application. Human body and bodily fluids have no effect on Ti and it is also compatible with bone growth (Bal Seal Engineering Inc., 2009). The as-received Ti-6Al-4V is cut from its bar into a dimension of 35mm×3mm×3mm using cutter (Figure 3.1) and lathe machine.

Table 3.1: Chemical composition of Ti-6Al-4V

Element	Titanium, Ti	Aluminum, Al	Vanadium, V	Carbon, C
Wt (%)	88.05	6.73	3.9	2.12

Bioactive HA powder supplied by Taihei Chemical Co. Ltd. Tokyo, Japan is used as the embedded material. HA coating on a metallic implant is very important so that the body would not see a foreign body and work in such a way as to isolate it from surrounding tissues. The average size of HA particles used is approximately 36.66 μm when (observed under FESEM)



Figure 3.1: Cutter

3.1.2 Sample Preparation

The heat treated Ti-6Al-4V is cut into a dimension of 35mm×10mm×3mm using cutter (Figure 3.1) as illustrated in Figure 3.2.

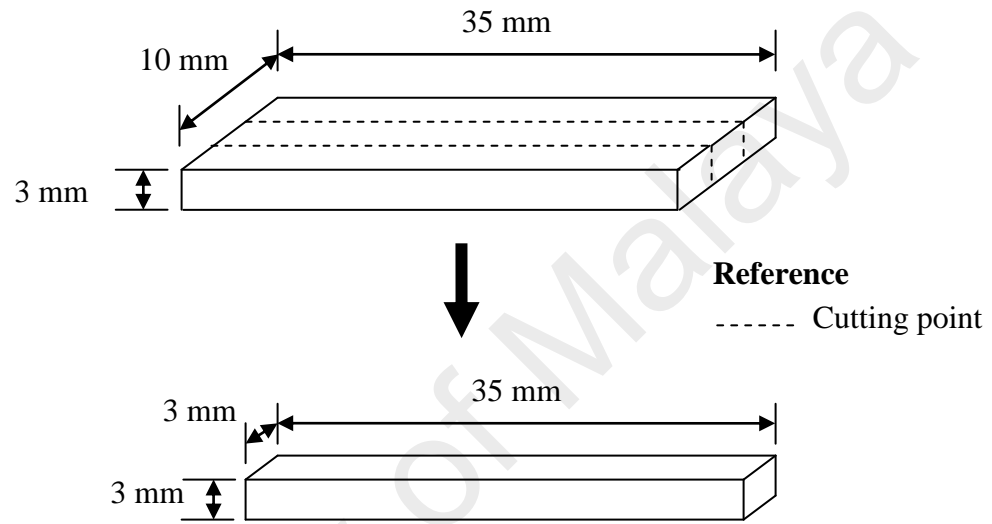


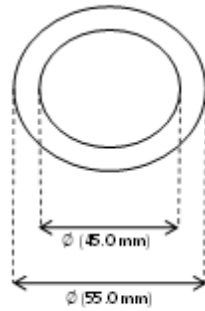
Figure 3.2: Dimension of the heat treated Ti-6Al-4V substrate before embedment

3.1.3 Die and Jigs Preparation

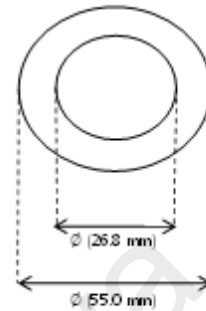
Embedment process needs special die and jigs made from high resistant stainless steel. Stainless steel has high temperature strength and excellent high temperature resistance to oxidation or scaling and therefore it is applicable for high temperature application. Figure 3.3 shows the design of die whilst Figure 3.4 depicts the fabricated die. Designs of jigs are shown in Figure 3.5. Both die and jigs are fabricated by using lathe and milling machine.

DIE:

TOP VIEW



BOTTOM VIEW



FRONT VIEW

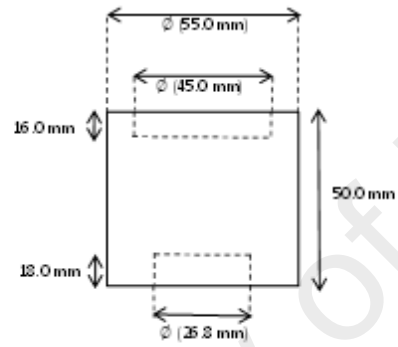


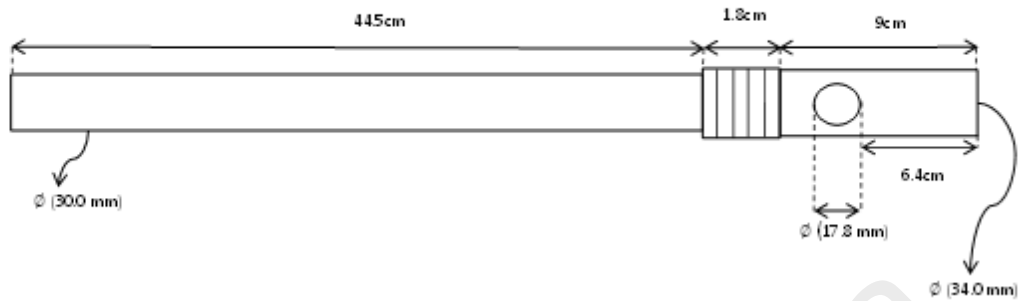
Figure 3.3: Design of die



Figure 3.4: Fabricated die

UPPER JIG:

FRONT VIEW



LOWER JIG:

FRONT VIEW

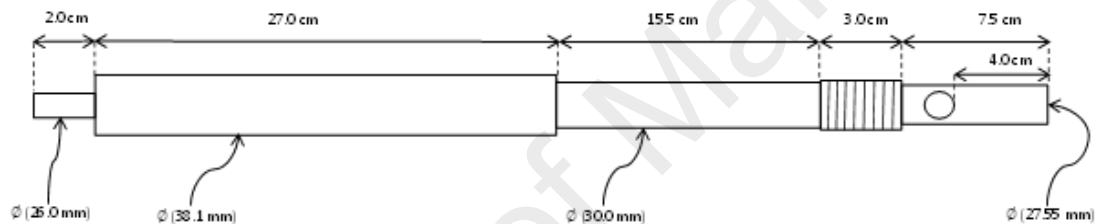


Figure 3.5: Design of jigs

3.2 Heat treatment

Prior to embedment process, the as-received Ti-6Al-4V with dimension of 35mm×3mm×3mm is solution-treated above the beta transus temperature (1373 K) for 30 minutes and ice-quenched to room temperature so that the globular, equiaxed alpha grains and beta phase in the as-received Ti-6Al-4V microstructure fully transform to martensitic alpha' phase (metastable phase), for the preparation of superplastic deformation. Figure 3.6 depicts the schematic diagram of the experimental setup for heat treatment process whilst Figure 3.7 illustrates the heat treatment profile. Removal of oxide layer and irregularities is done by polishing the sample on emery paper up to 1200 grit size.

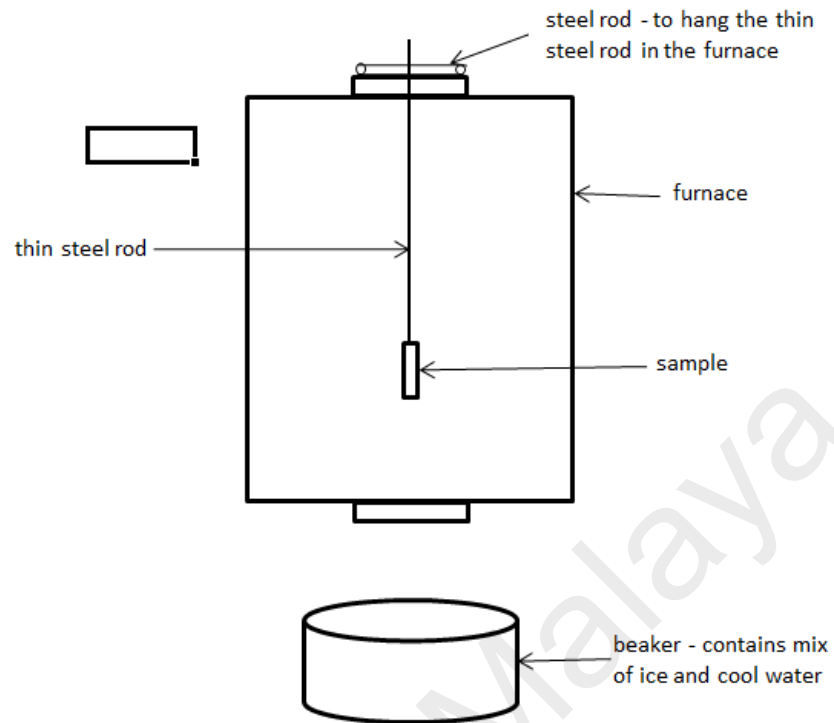


Figure 3.6: Schematic diagram of the experimental set-up for heat treatment process

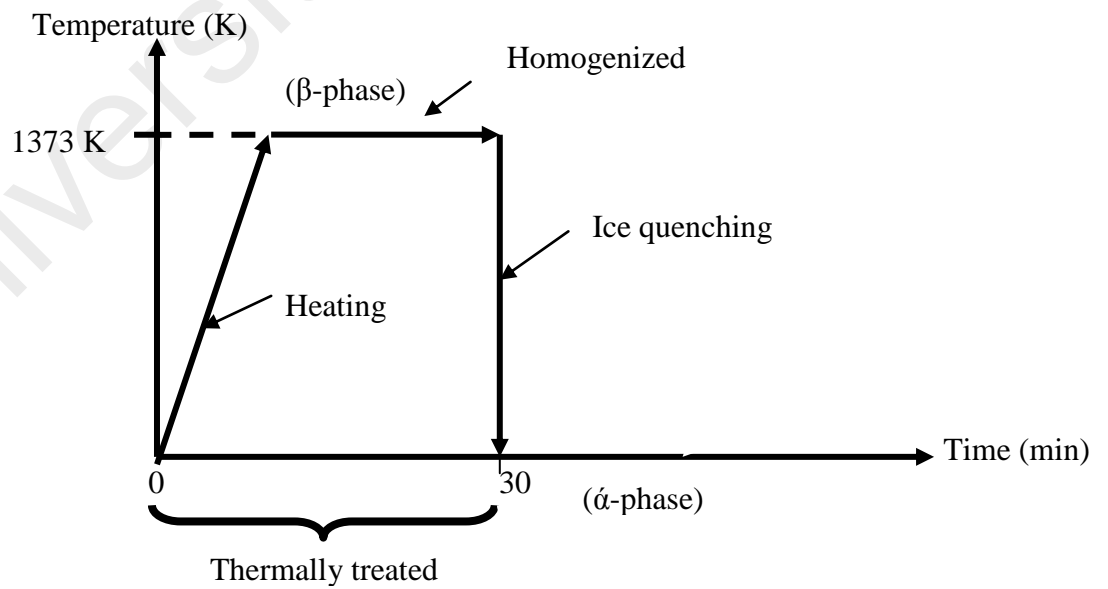


Figure 3.7: Heat treatment profile of Ti-6Al-4V

3.3 Embedment process

Superplastic embedment is carried out by compression test machine equipped with high temperature furnace under Argon controlled atmospheric condition at 927 °C. Argon gas is used to prevent the oxidation of die and jigs at high temperature. Placement of the Ti-6Al-4V and HA powder in the fabricated die is shown in Figure 3.8 and Figure 3.9. The entire schematic diagram of the experimental set-up in the compression machine is demonstrated in Figure 3.10. Movable crosshead must be placed align with the fixed crosshead so that compression force can be evenly distributed throughout the samples and thus, resulting in uniform contact between substrate's surface and HA powder.

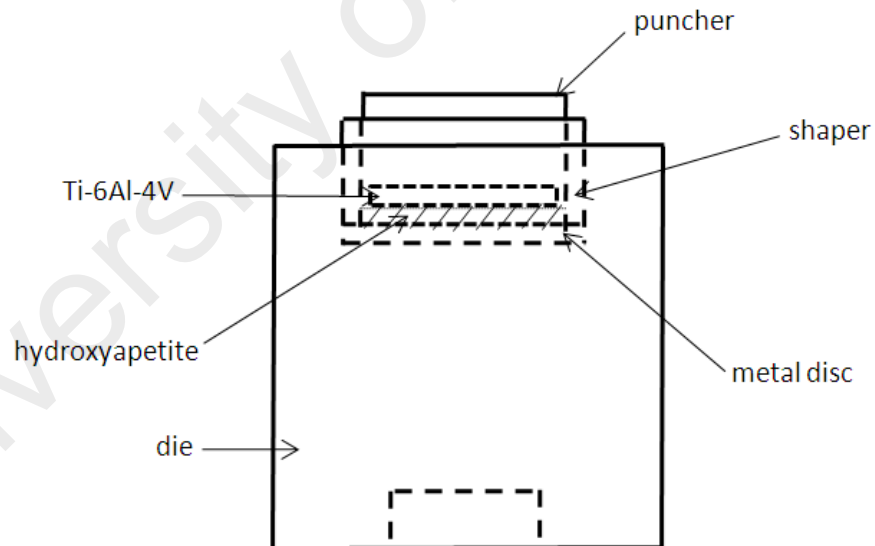


Figure 3.8: Front view illustration of Ti-6Al-4V and HA powder in the die



Figure 3.9: Fabricated die with the Ti-6Al-4V substrate and HA powder inside it, to be placed in the compression test machine for embedment process

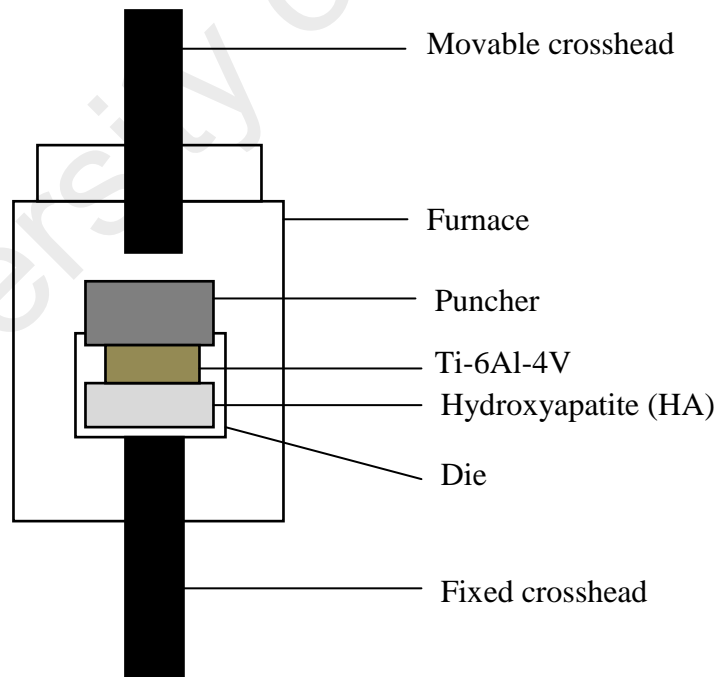


Figure 3.10: Schematic diagram of experimental set-up in the compression machine

Samples is heated from room temperature to 927 °C and kept at this temperature for 1 hour to ensure thermal equilibrium before embedment process. Sample is pressed by the upper jigs with compression strain rate of $1 \times 10^{-4} \text{ s}^{-1}$ until achieving 54 % deformation. Several deformations have been tested and 54% is found to be the maximum deformation for Ti-6Al-4V. The entire embedment profile is illustrated in Figure 3.11.

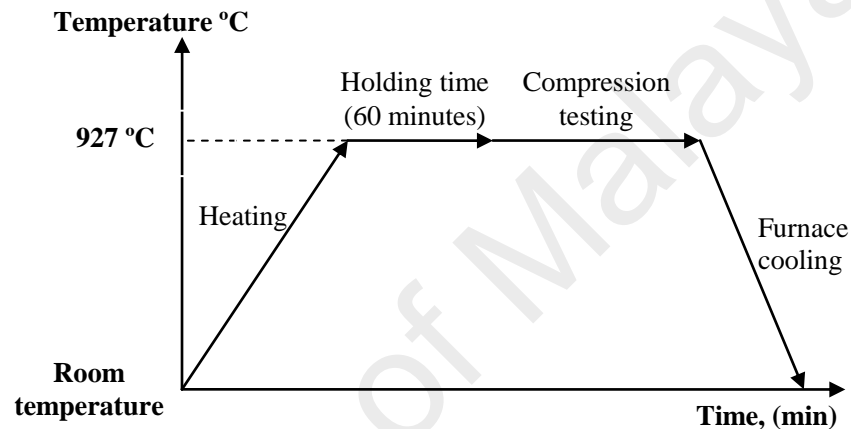


Figure 3.11: Superplastic embedment profile

3.4 Bioactivity test

After being cleaned with alcohol, rinsed with distilled water, each sample is placed in a closed container which contains 20 ml SBF (Figure 3.12) and kept in a furnace at constant temperature of 37°C (Figure 3.13) for 1, 3, 7, 14, 21, 28 and 35 days without stirring. The embedded surface should be facing up the lid to ensure that the entire surface will be fully exposed to SBF (Kokubo and Takadama, 2006). SBF is a useful solution which has ion concentration nearly identical to human blood plasma to predict the in vivo bioactivity of a material based on the bone-like apatite formation on its surface in SBF

(Kokubo, 1991). Prior to characterization assessments of the HA layer, samples are rinsed with distilled water and dried at room temperature.



Figure 3.12: Embedded sample immersed in the 20 ml SBF



Figure 3.13: Sample in SBF is placed in the furnace at constant temperature of

37 °C

3.5 Nanoscratch test

The mechanical properties of the layer before and after application in SBF are determined through adhesion strength measurements using Micro Materials NanoTest (Wrexam, UK) nanoscratch testing platform (Figure 3.14). Figure 3.15 depicts the position of the sample which must be placed opposite to the pendulum. Even though there are more than 250 methods available to evaluate the mechanical properties (Mittal, 1995), however scratch test is the simplest (Toque et al., 2010) and laudable way especially for hard coating application (Rickerby, 1988; Valli, 1986). This technique involves generating a controlled scratch with a sharp tip on the selected area of a sample. The tip material (commonly diamond or hard metal (tungsten carbide) is drawn across the coated surface under constant, incremental or progressive load. At a certain critical load, the coating will start to fail. Figure 3.16 schematically illustrates the scratching done by indenter on a sample.

In this experiment, a conical diamond indenter is used to produce scratches by linearly increasing load up to four maximum scratch loads: 50 mN, 100 mN, 300 mN and 500 mN. The scratching length is fixed to 1000 μm .

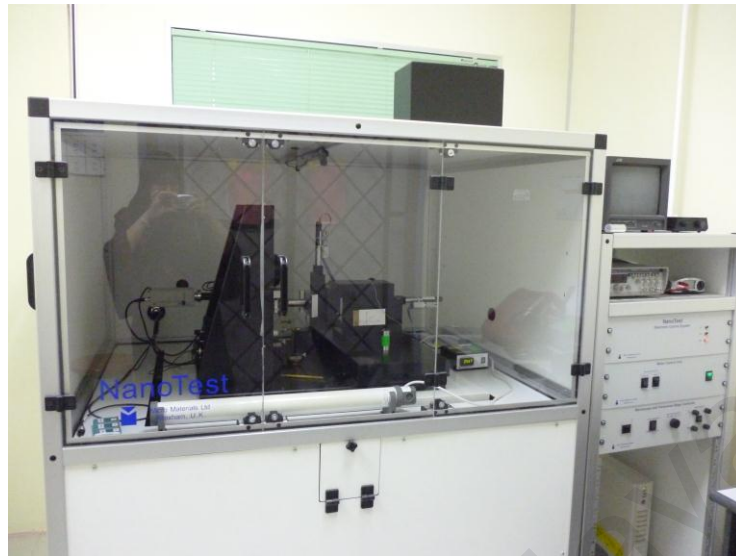


Figure 3.14: Nanoscratch testing machine

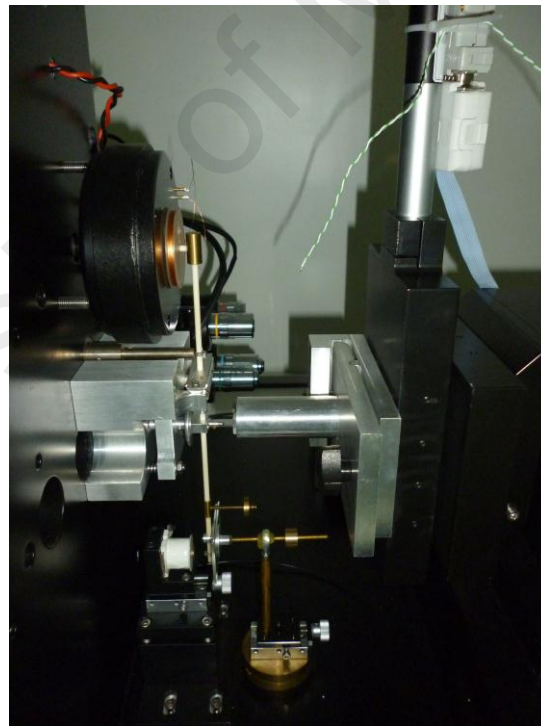


Figure 3.15: Position of the sample and pendulum

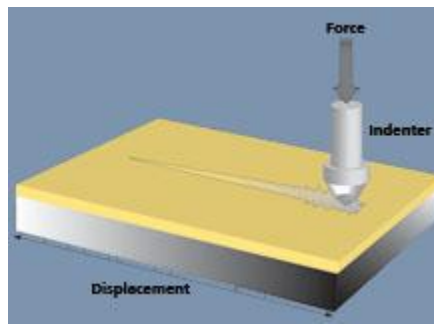


Figure 3.16: Scratching illustration on the coating

3.6 Microhardness Test

Hardness is the measure of how resistant solid matter is to various kinds of permanent shape change when a force is applied. It measures the resistance of a sample to permanent plastic deformation due to a constant compression load from a sharp object. Hardness is dependent on ductility, elastic stiffness, plasticity, strain, strength, toughness, viscoelasticity and viscosity. Microhardness equipment comprises a range of light loads and a precision diamond indenter. A square base pyramid shaped diamond indenter is for the application in Vickers scale and a narrow diamond shaped indenter is for the application in Knoop scale. Microhardness equipment usually has magnification of around 500 times and measure to accuracy of ± 0.5 mm (Gordon England, 2008).



Figure 3.17: Microhardness tester

In this research, the hardness of the HA layer and Ti-6Al-4V substrate is measured by Mitutoyo MK-17 series microhardness tester (Figure 3.17) with an applied load of 2N and loading time of 10s.

3.7 Characterization process

After embedment and immersion in the SBF, FESEM (Zeiss) is used to characterize the microstructure of the HA embedded layer and to study its microscopic properties. Elemental composition of the layer is identified by EDX analysis. Details of the crystallographic structure of the layer are revealed by XRD (X Pert PRO).

3.7.1 Field Emission Scanning Electron Microscope (Zeiss FESEM)

FESEM is a major tool in materials science research and development. FESEM includes a source of electrons; lenses which are focused to a fine beam; arrangement for detecting electrons emitted by the specimen; and an image display system (Goldstein et al, 2003).

Under vacuum, electrons generated by a field emission source are accelerated in a field gradient. The electron beam passes through electromagnetic lenses, focusing onto the specimen. As result of this bombardment different types of electrons are emitted from the specimen. A detector catches the secondary electrons and an image of the sample surface is constructed by comparing the intensity of these secondary electrons to the scanning primary electron beam. In the FESEM, a relatively large sample can be used and rather large areas observed (Brooks and Choudhury, 1993). The image is finally displayed on a monitor. For using FESEM, conductive samples (Goldstein et al., 2003) are generally mounted rigidly on a specimen holder called a specimen stub and must be of an appropriate size to fit in the specimen chamber.

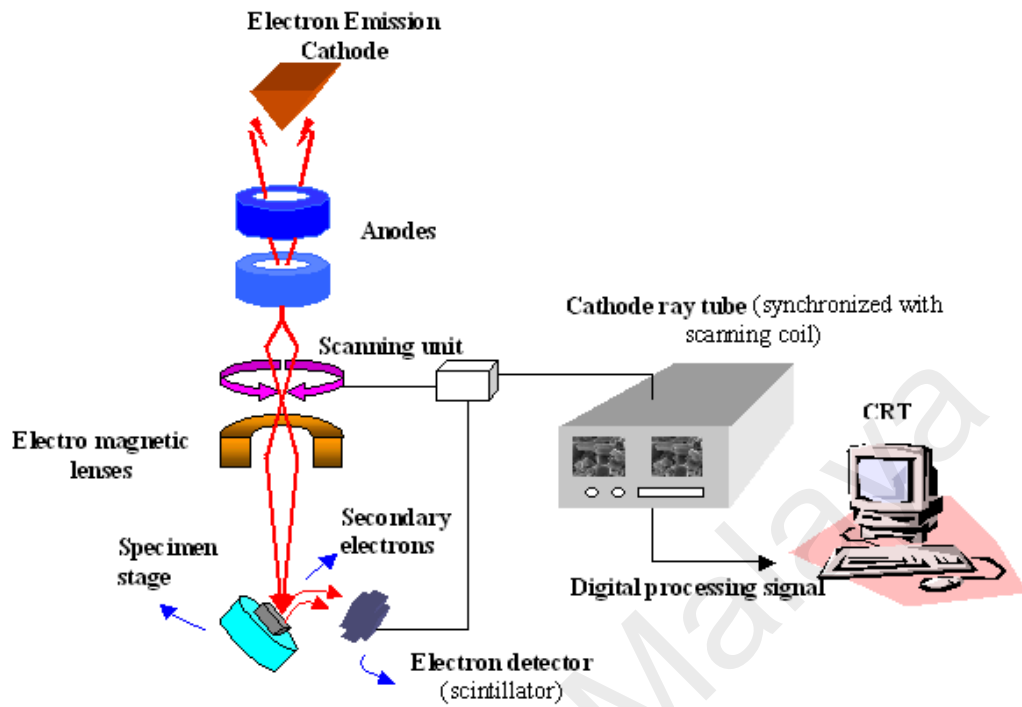


Figure 3.18: FESEM principle

In comparison to the conventional scanning electron microscope (SEM), FESEM produces clearer and less electrostatically distorted images with spatial resolution down to 1.5 nm which is 3 to 6 times better than SEM.



Figure 3.19: FESEM

In this research, Zeiss FESEM (Figure 3.19), operating with an accelerating voltage below 6 kV is used to characterize the surface morphology of embedded layer and to determine layer thickness.

3.7.2 Energy Dispersive X-Ray (EDX) Analysis

EDX analysis is an x-ray technique used to identify the elemental composition of materials. EDX detector combined with digital image processing is a powerful tool in the study of materials, allowing good chemical analysis of the material. It relies on the investigation of an interaction of some source of X-ray excitation and a sample. Some of the EDX applications are in materials and product research, troubleshooting and deformation. EDX systems are attached to SEM/FESEM and Transmission Electron Microscopy (TEM) instruments where the imaging capability of the microscope identifies the specimen of interest. There are four primary components of EDX: beam source, X-ray detector, pulse processor and the analyzer (Materials Evaluation and Engineering, Inc., 2009). Figure 3.20 shows the schematic diagram of EDX working system. The data generated by EDX analysis consist of spectra showing peaks corresponding to the elements making up the true composition of sample being analyzed. In a multi-technique approach EDX becomes very powerful, particularly in contamination analysis and industrial forensic science investigations. The technique can be qualitative or semi-quantitative or quantitative and it provides spatial distribution of elements through mapping. The EDX technique is non-destructive and specimens of interest can be examined in situ with little or no sample preparation. Benefits of using EDX analysis are:

- Improved quality control and process optimization
- Rapid identification of contaminant and source
- Full control of environment factors, emission and many more
- Greater on-site confidence, higher production yield
- Identifying the source of the problem in process change

In this research, the elemental composition of layer is identified and measured by EDX analysis.

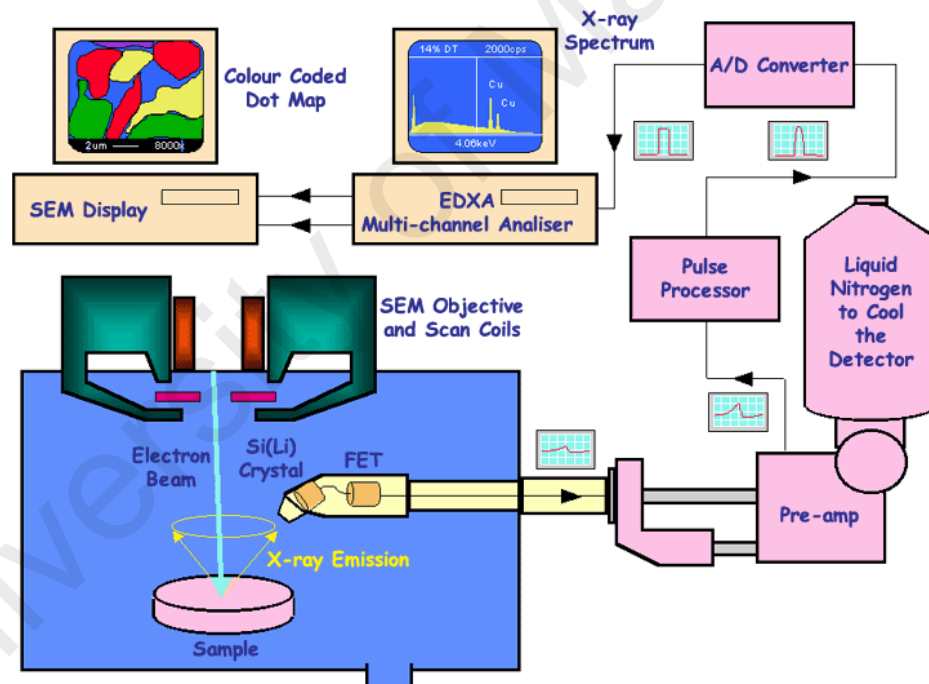


Figure 3.20: Schematic diagram of EDX working system

3.7.3 X-Ray Diffraction (XRD)

Diffraction occurs when a wave encounters a series of regularly spaced obstacles that (1) are capable of scattering wave, and (2) have spacings that are comparable in magnitude to the wavelength (Callister, 2007). Since most materials have unique diffraction patterns, compounds can be identified by using a database of diffraction patterns. The purity of a sample can also be determined from its diffraction pattern, as well as the composition of any impurities present. A diffraction pattern can also be used to determine and refine the lattice parameters of a crystal structure. XRD is a powerful technique used to characterize crystalline materials. The crystals that make up a crystalline material have unique dimensions that are characteristic of a material. Using an x-ray diffractometer, and Bragg's law the crystallography of a material can be determined. A crystal lattice is a regular three-dimensional distribution (cubic, rhombic, etc.) of atoms in space. These are arranged so that they form a series of parallel planes separated from one another by a distance d , which varies according to the nature of the material. For any crystal, planes exist in a number of different orientations - each with its own specific d -spacing. When a monochromatic x-ray beam with wavelength λ is projected onto a crystalline material at an angle θ , diffraction occurs (Figure 3.21) only when the distance traveled by the rays reflected from successive planes differs by a complete number n of wavelengths.

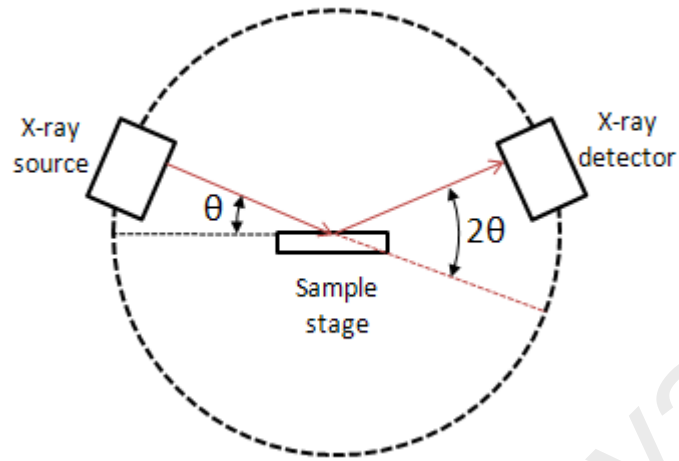


Figure 3.21: XRD working system

By varying the angle theta, the Bragg's Law conditions are satisfied by different d -spacings in polycrystalline materials. Plotting the angular positions and intensities of the resultant diffracted peaks of radiation produces a pattern, which is characteristic of the sample. Where a mixture of different phases is present, the resultant diffractogram is formed by addition of the individual patterns. Based on the principle of x-ray diffraction, a wealth of structural, physical and chemical information about the material investigated can be obtained.



Figure 3.22: XRD equipment

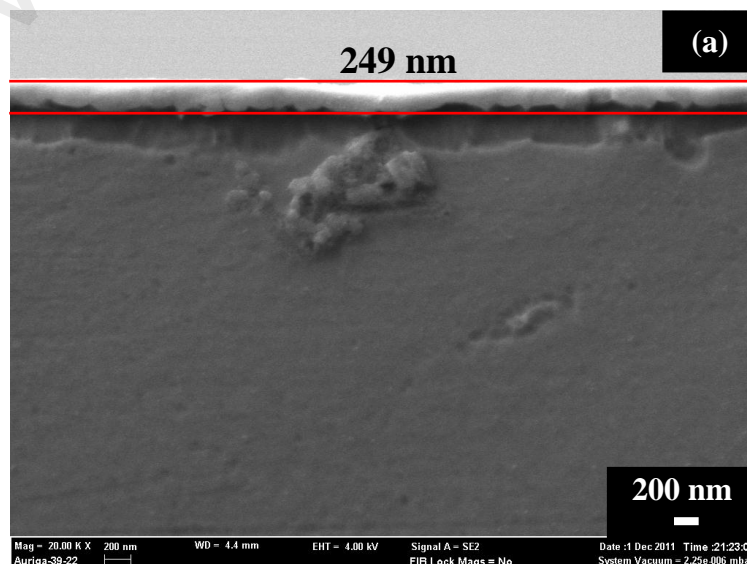
In this research, detailed information about the chemical composition and crystallographic structure of the layer are revealed by XRD (X Pert PRO) analysis (Figure 3.22).

CHAPTER 4

RESULTS AND DISCUSSION

4.1 Properties of the HA Embedded Layer and Its Characterizations

HA embedded layer of 249 nm average thickness of cross section of the sample (Figure 4.1(a)) with an average layer hardness of 660 HV is obtained after superplastic embedment. Surface morphology of HA embedded layer observed under FESEM at low magnification in Figure 4.1(b), indicates that the surface is rough and dense. Under high magnification Figure 4.1(c), the nonadjacent, nonparallel and overlapped arrangement of a needle-like HA crystal is observed, together with the significant amount of pores. This surface morphology is able to support tissue adhesion and growth and reduces problems associated with stress shielding because of the ability to control its elastic modulus to match that of bone (Das et al., 2008).



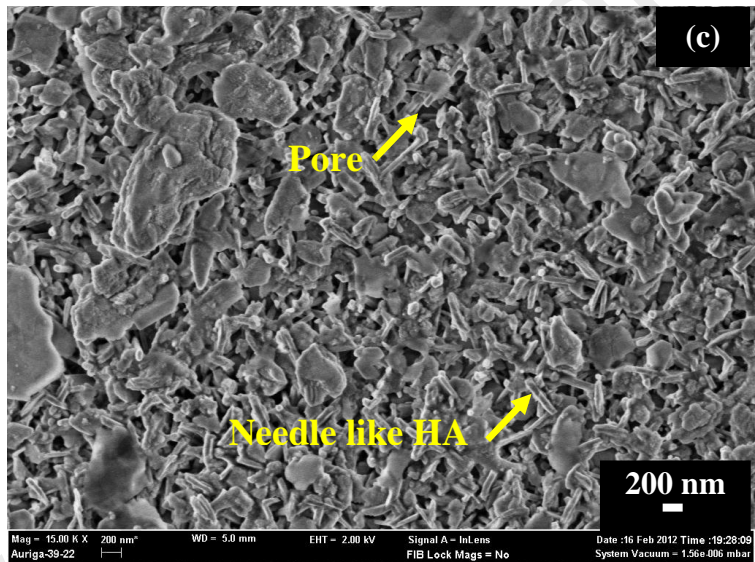
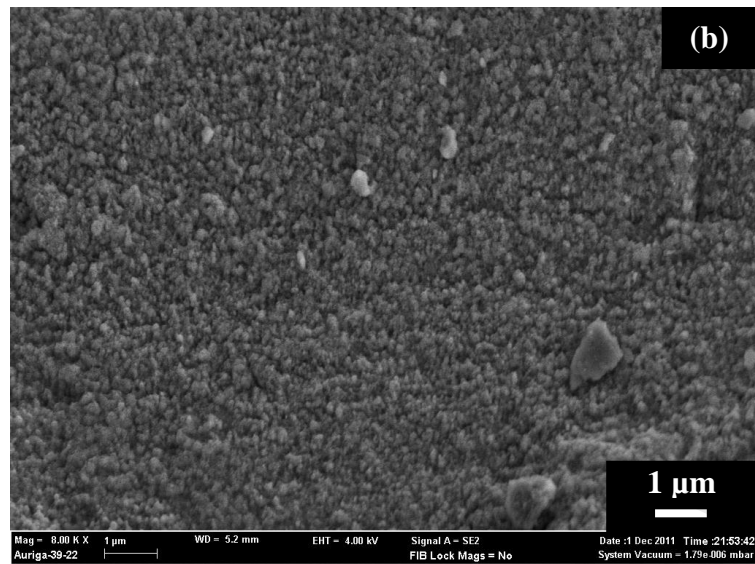


Figure 4.1: FESEM image of the (a) cross section (b) surface morphology at 8000 magnification and (c) surface morphology at 15000 magnification of an HA embedded layer

HA embedded layer also consists of Ti element as shown in EDX analysis (Figure 4.2). The presence of Ti element in the HA embedded layer is important to achieve good adhesion between the embedded layer and the substrate. Adhesion between the layer and the substrate should be sufficiently high so as to endure the interfacial stresses encountered in

the in vivo environment where bone ongrowth occurs on the bioactive surface provided by the HA embedded layer. Ti element could help to grip the HA particles firmly and thus provide good cohesive strength between particles in the embedded layer. It also offers strong adhesive strength between the HA embedded layer and the substrate (Khalid et al., 2012). Thus, superplastic embedment can be considered as an impeccable chosen method which produces a good mixture of a sufficient amount of calcium (Ca), phosphorus (P) and Ti elements in the embedded layer without the need for a peripheral mixing process.

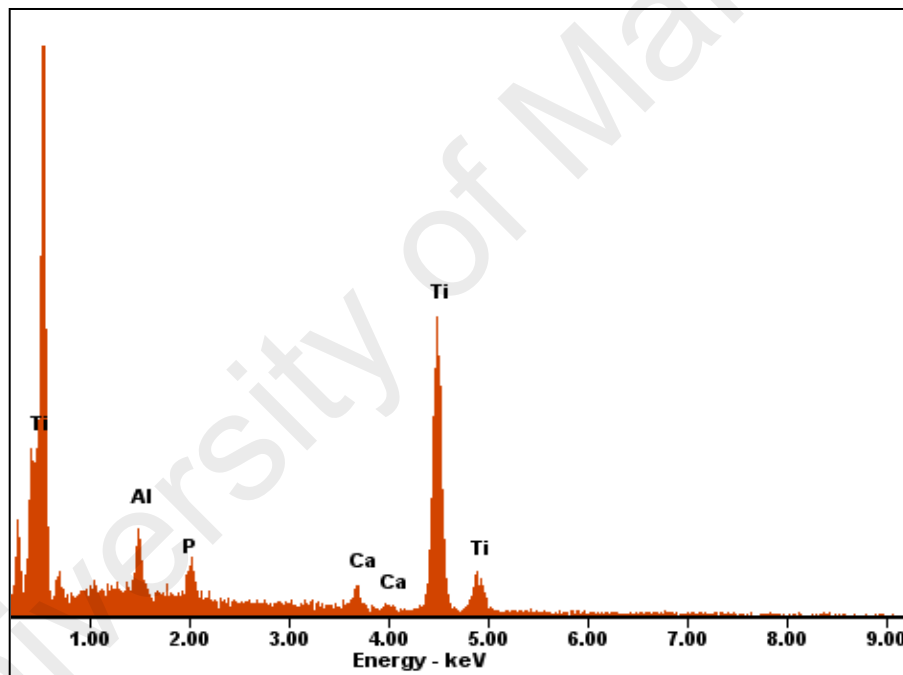


Figure 4.2: EDX spectrum on surface morphology of an HA embedded layer

Table 4.1: Elemental percentage of the EDX spectrum (Figure 4.2) on surface morphology of an HA embedded layer

Element	Wt %	At %
AlK	3.57	6.05
PK	2.46	3.63
CaK	2.76	3.15
TiK	91.22	87.17

In comparison to the Ti alloy average surface hardness of 433 HV, the significant increment in surface hardness suggests that a dense layer has successfully formed. The maximum stress of about 184 MPa (Figure 4.3) applied in the embedment process assists in the density of the layer (Khalid et al., 2012). Further, the substrate's fine grains assist in mutual diffusion of HA and Ti, generating good adhesion strength between the layer and the substrate.

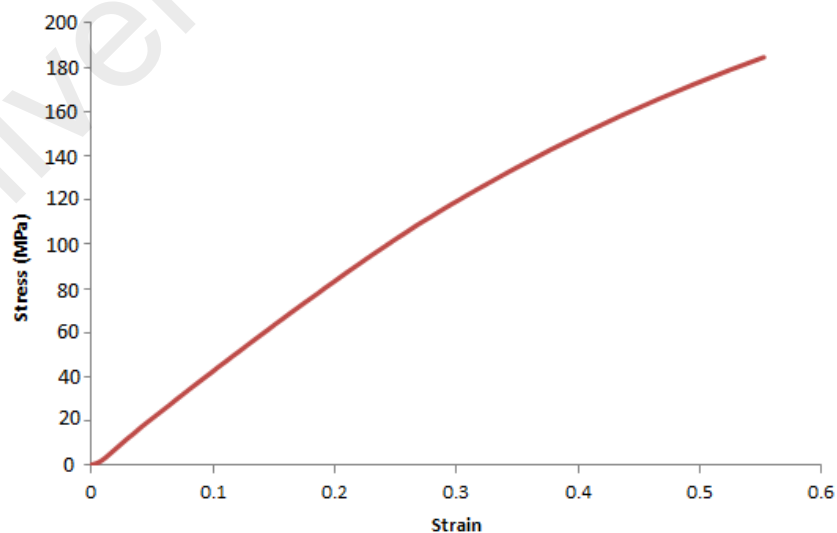
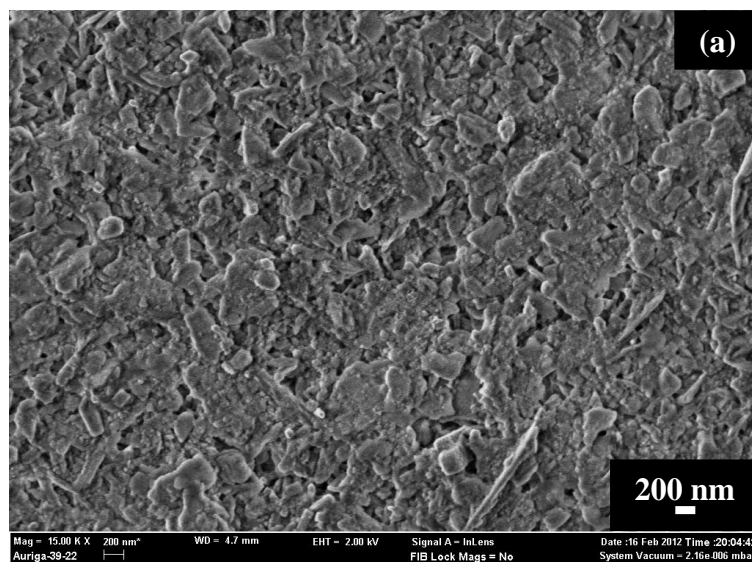
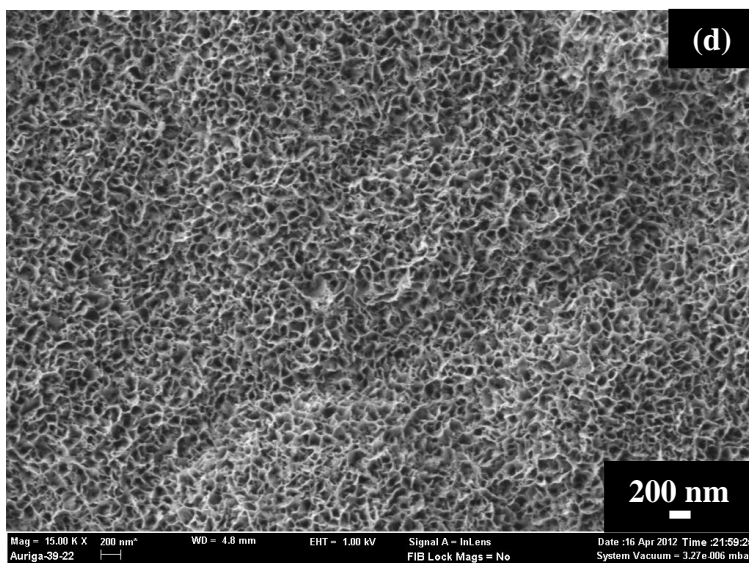
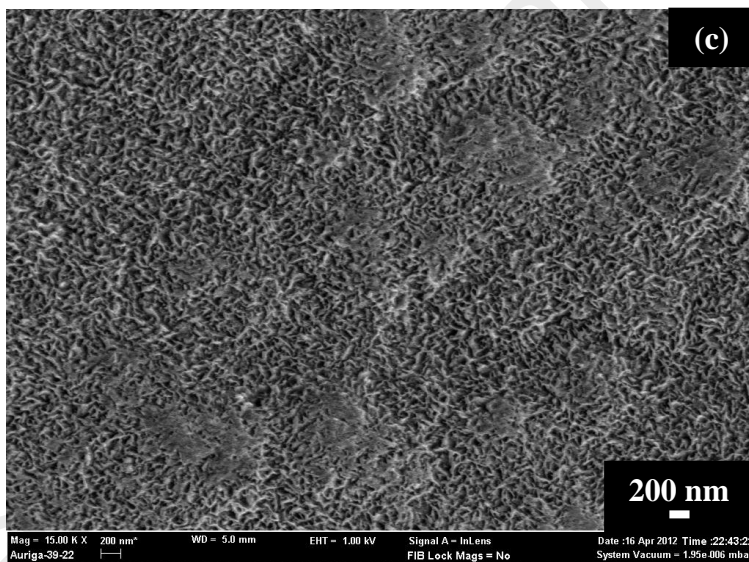
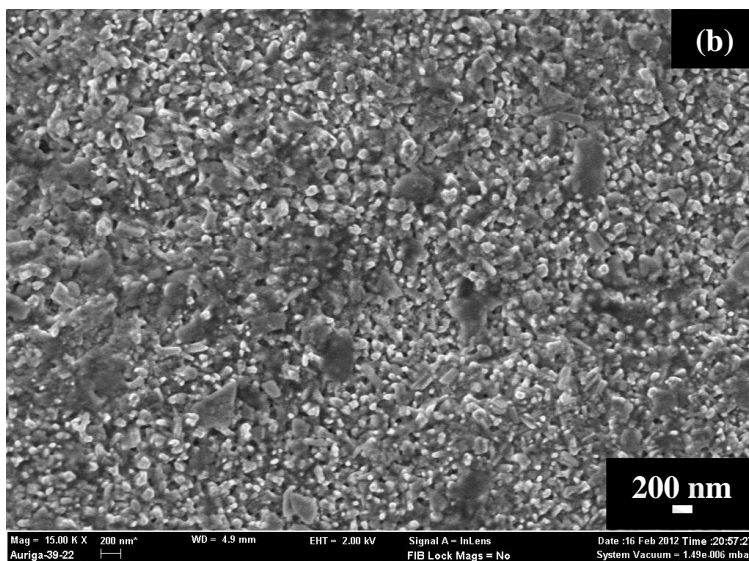


Figure 4.3: Stress-strain relationship during embedment process

4.2 Bioactivity of the HA Embedded Layer

Bioactivity defines the ability of bone-like apatite layer to grow on a sample. Bioactivity is one of the requirements for biocompatibility besides harmless properties. The surface morphologies of the embedded layer after soaking in SBF for various periods of time are shown in Figure 4.4(a-g). After 1 day of immersion, the surface morphology of the HA layer remains unchanged (Figure 4.4(a) - refer Figure 4.1(c)). However, thickness of about 11 nm of the newly grown HA layer is observed (Figure 4.5). Pores are still identified on the layer surface at this stage, but the amount is less compared to those on the surface of non-immersed samples. After 3 days of immersion, the average thickness of the newly grown HA layer increases up to 30.1 nm. Pores are filled with the precipitation of HA particles, where the HA precipitates are observed growing out from the pores (Figure 4.4(b)). The porous surface of the implant is important to allow bone ingrowth and thus promote bone regeneration (Ahmed and Jankowski, 2011). More pores provide more nucleation sites for a bone-like apatite layer.





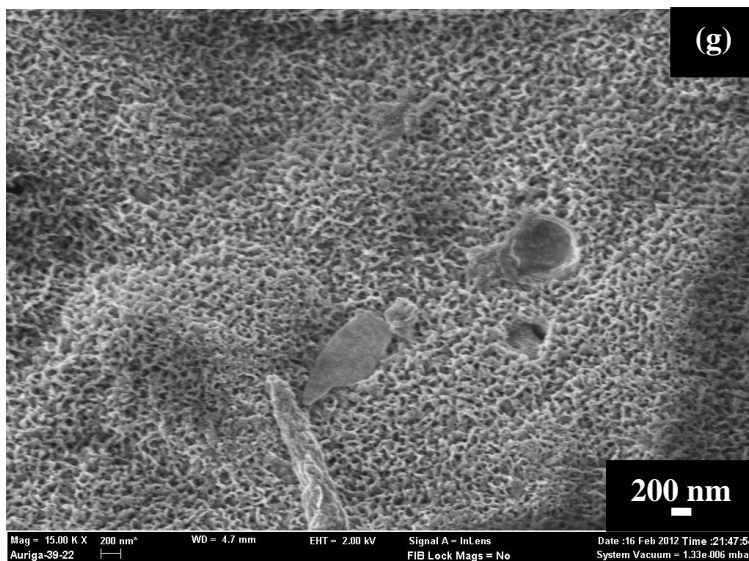
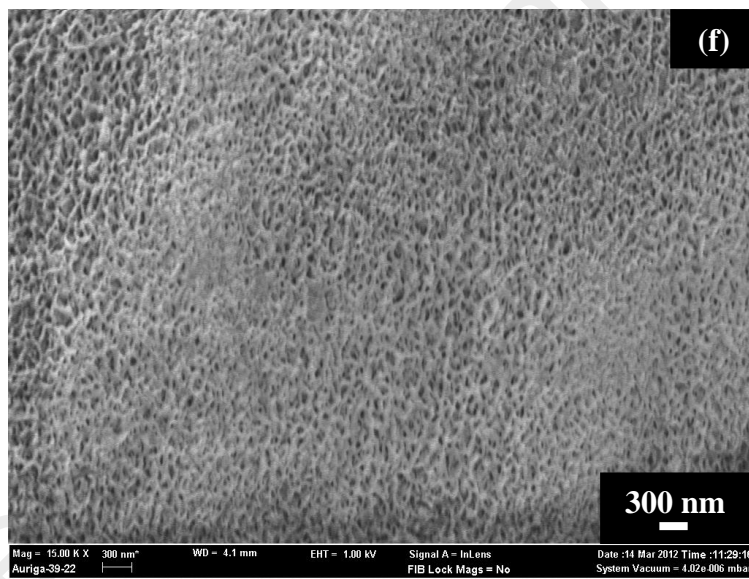
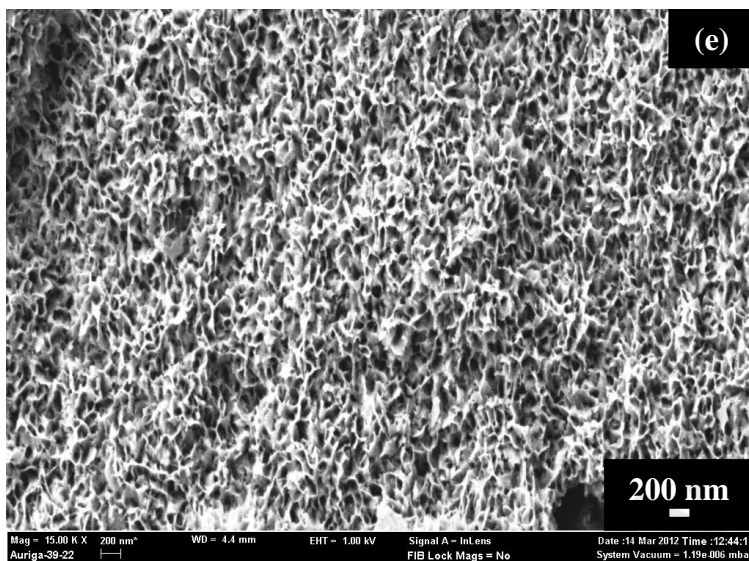


Figure 4.4: FESEM image of surface morphology of the HA layer after immersion in SBF for (a) 1 day, (b) 3 days, (c) 7 days, (d) 14 days, (e) 21 days, (f) 28 days and (g) 35 days

The three-dimensional mesh-like structure is formed after 7 days of immersion and the obtained microstructure is almost similar to bone (Figure 4.4(c)). The average thickness of the newly grown HA layer at this stage is 64.3 nm. This phenomenon indicates that the exposed zone of newly grown HA precipitates also act as favored nucleation sites. After 14 days of immersion, the embedded layer is fully covered with a newly grown bone-like apatite layer of 86 nm average thickness (Figure 4.4(d)). The thickness of the newly grown HA layer becomes greater for the subsequent 21, 28 and 35 days of immersion, which amount to approximately 100, 152.9 and 242.3 nm, respectively. After 35 days of immersion, the thickness of the newly grown HA layer is as thick as the original embedded layer. The constructive growth in thickness of the newly grown HA layer and changes in the surface morphology of the layer shows that the exposed zone of newly grown HA layer also act as a favored nucleation sites where HA elements from the SBF keep precipitate to form bone-like apatite layer. This is a significant indication of its bioactivity for use in the human body.

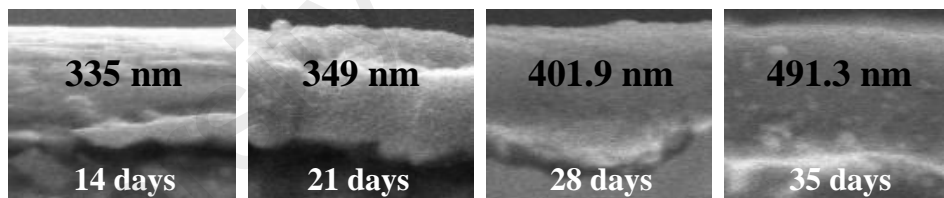
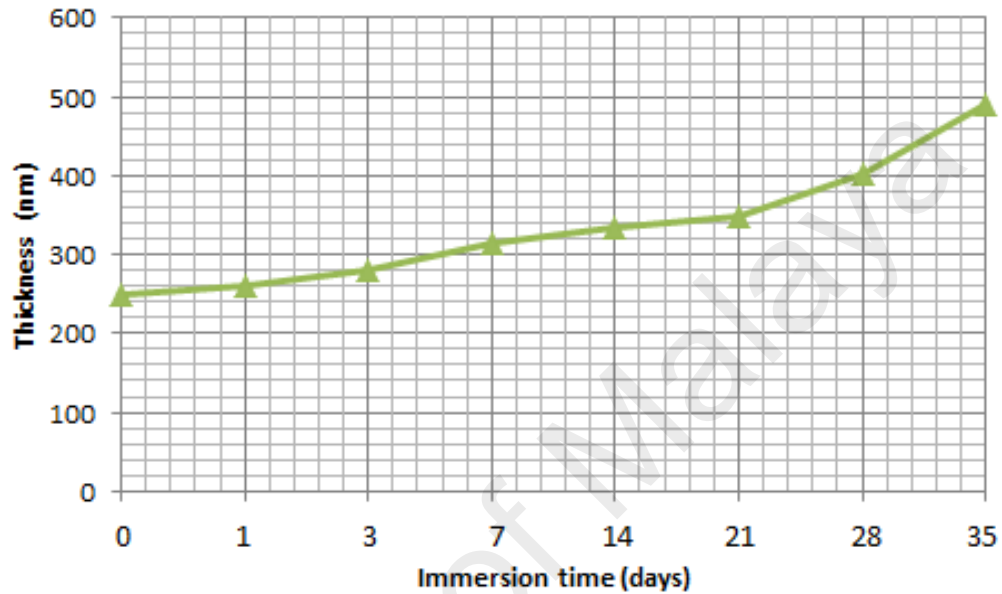
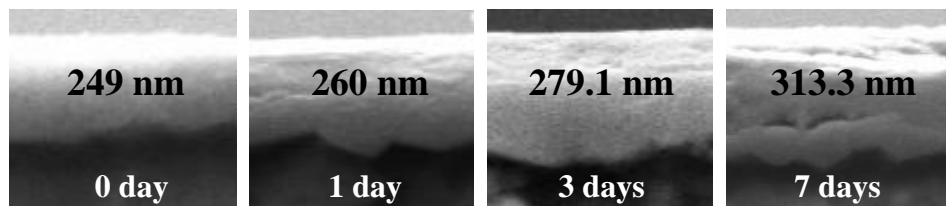


Figure 4.5: Average thickness of the HA layer at different immersion time in SBF

As seen from Figure 4.5, the increment in thickness of the newly grown HA layer is observed right from the beginning of immersion and it increases at a much higher rate after 21 days. Despite having nanosize thickness, the amount of HA elements in the superplastically embedded layer is sufficient for the formation of a carbonate apatite layer in SBF. The increment of XRD peaks from day 0 to day 35 of immersion, as reflected in Figure 4.6(a-i), which indicates the growth of HA particles on the embedded layer and thus proves its bioactivity.

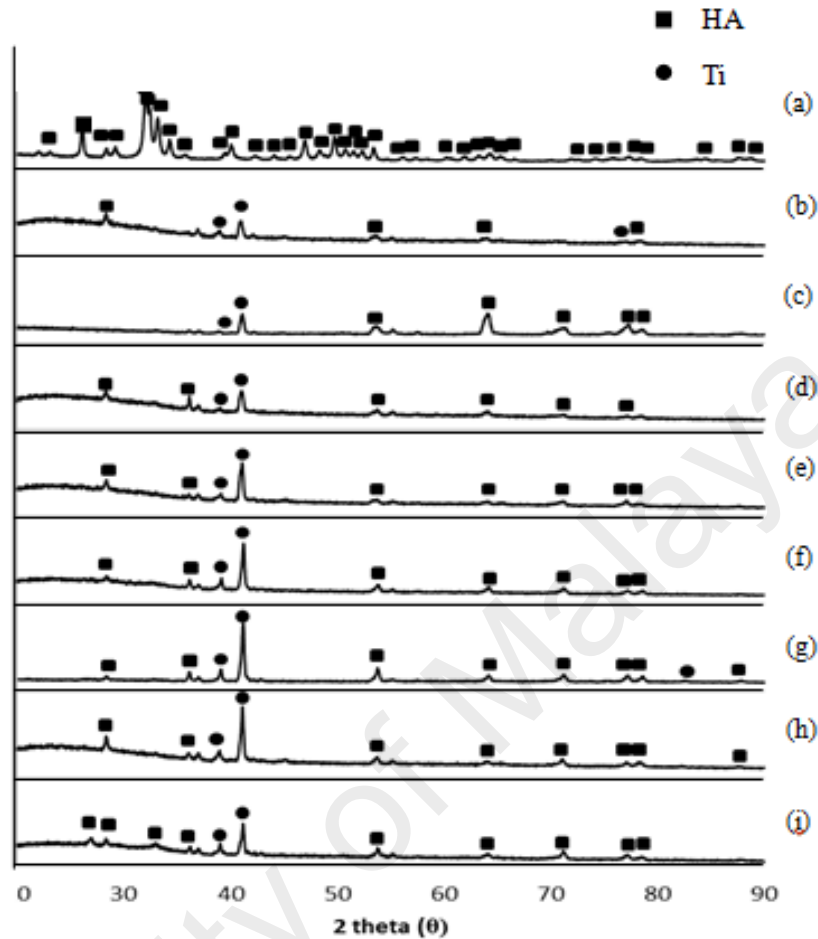


Figure 4.6: XRD pattern of (a) pure HA powder and the HA layer after (b) 0 day (c) 1 day (d) 3 days (e) 7 days (f) 14 days (g) 21 days (h) 28 days (i) 35 days of immersion in SBF

The hardness of the HA layer is observed to decrease from day 1 to day 35 of immersion (Figure 4.7). The hardness in the early stages is influenced by the hardness of the original embedded layer of average 660 HV which is denser and richer in the Ti element. Consequently, the average hardness of the layer from day 1 to day 3 remains relatively high, being 654 HV and 648 HV, respectively. For the following days of immersion, when the newly grown HA layer becomes thicker and contains a higher amount of pores, the effect of hardness of the original embedded layer lessens. Hence, this leads to

a greater decrease in hardness. Amounts of hardness after 7, 14, 21, 28 and 35 days are about 640 HV, 638 HV, 626 HV, 596 HV and 580 HV, respectively.

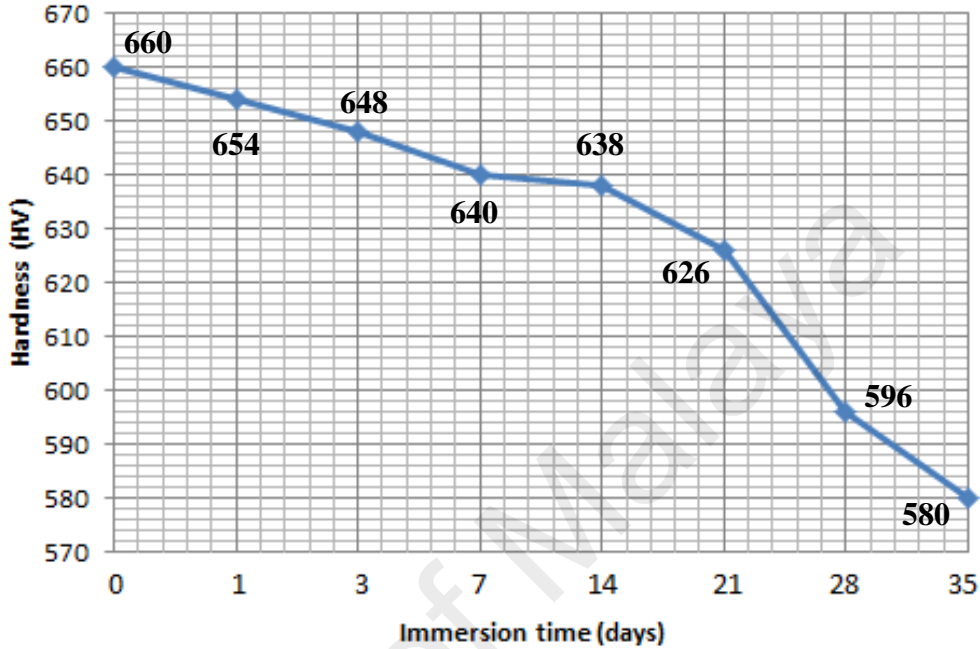


Figure 4.7: Hardness of the HA layer at different immersion time in SBF

4.3 Nanoscratch Properties of the HA Embedded Layer

The indenter tip slides over the layer with increasing scratch load and causes the peeling-off of the newly-grown HA layer in the form of flakes, as shown in the typical scratch track in Figure 4.8.

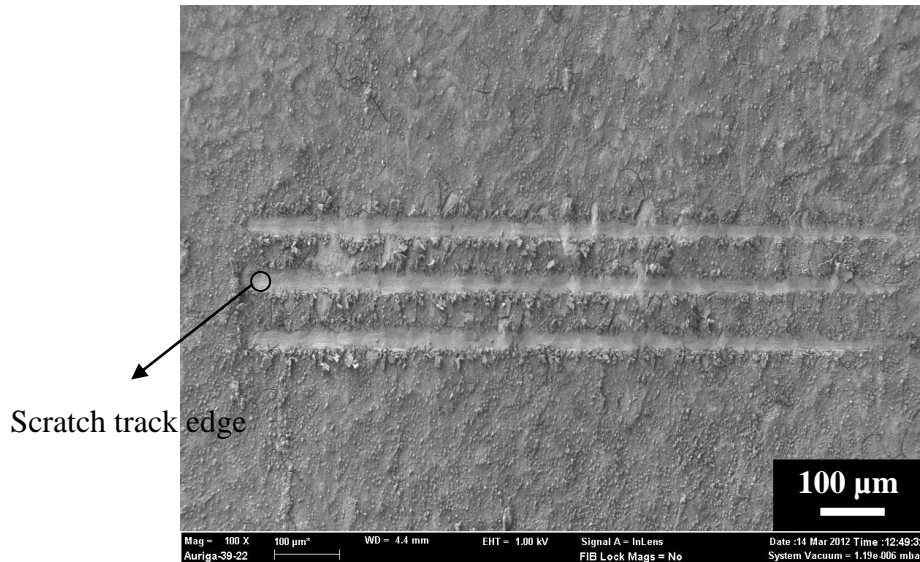
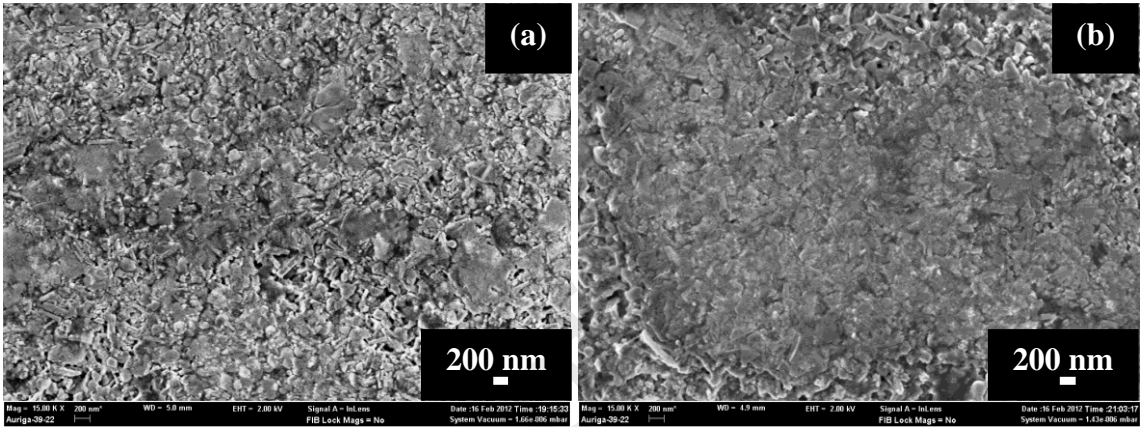


Figure 4.8: FESEM image of 1000 μm length scratch track, scratched with 500 mN scratch load on a sample immersed for 7 days in SBF

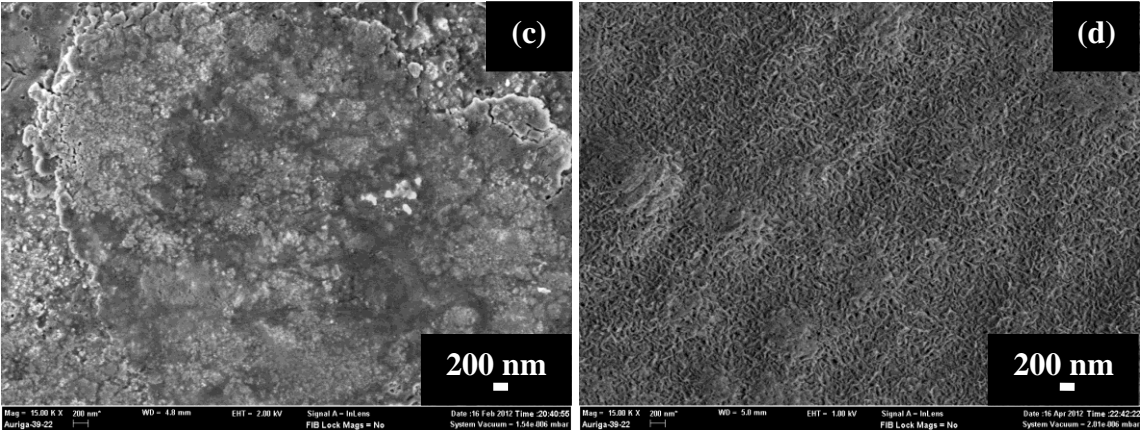
Delamination of the surface increases and becomes more apparent towards the sliding direction up to the edge of the scratch track with the increase in the scratch load. The scratch track edge (circled area) in Figure 4.8 is magnified and further analyzed. The results for each sample at different immersion conditions are presented in Figure 4.9(a-h), Figure 4.10(a-h), Figure 4.11(a-h) and Figure 4.12(a-h). From the figures, the effects of scratch loads become more evident at higher scratch load and longer immersion time in SBF.

The lowest scratch load of 50 mN has almost no effect on the HA embedded layer (Figure 4.9(a)) due to the strong cohesive strength provided by the strong grip between Ti element and HA particles. The surface is almost totally flattened after 21 days of immersion in SBF (Figure 4.9(f)) and is fully flattened after 28 days (Figure 4.9(g)) under 50 mN scratch load. Scratch grooves start to reveal after 21 days (Figure 4.9(f)) and becomes more obvious after 28 (Figure 4.9(g)) and 35 days (Figure 4.9(h)).



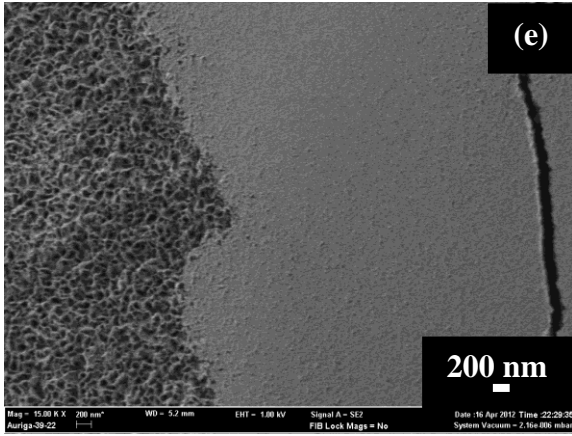
0 day

1 day

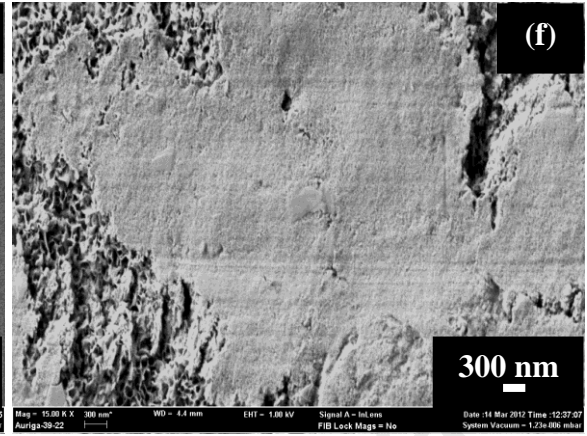


3 days

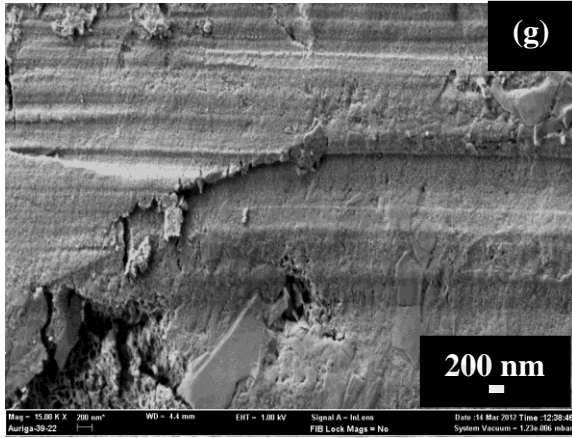
7 days



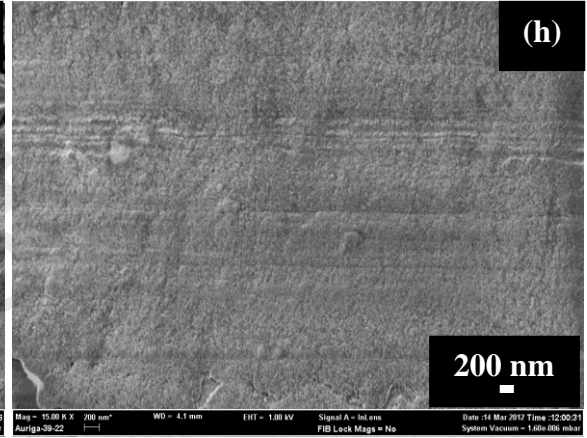
14 days



21 days



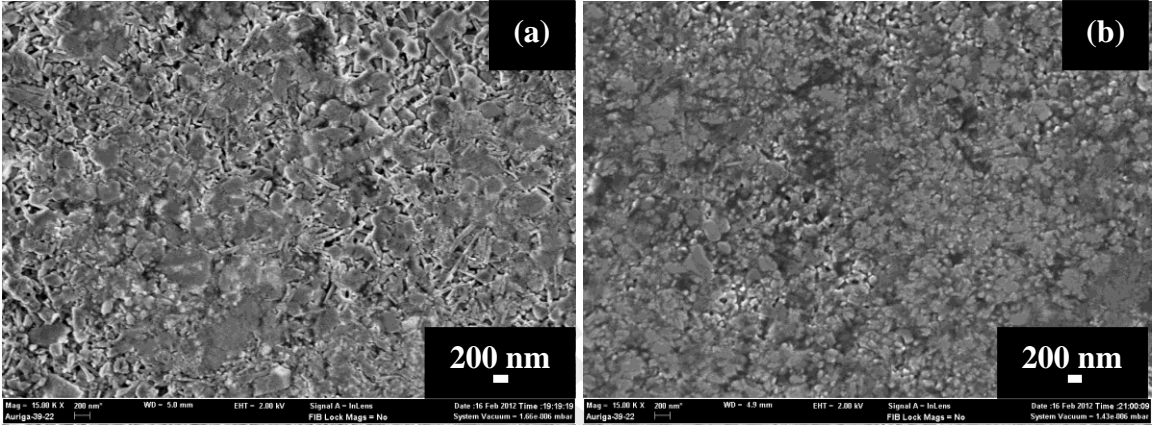
28 days



35 days

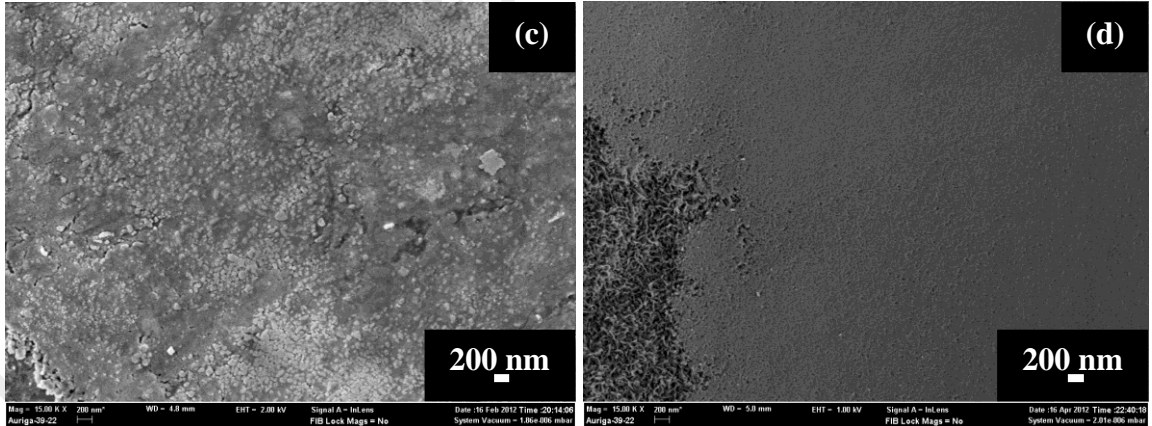
Figure 4.9: FESEM images of the end of scratch track scratched at 50 mN load (15 k magnification)

At the higher scratch load (100 mN), the surface is almost totally flattened after 7 days of immersion in SBF (Figure 4.10(d)) however without reaching the original HA embedded layer. Scratch grooves are revealed after 21 days (Figure 4.10(f)) and become more obvious after 28 (Figure 4.10(g)) and 35 days (Figure 4.10(h)).



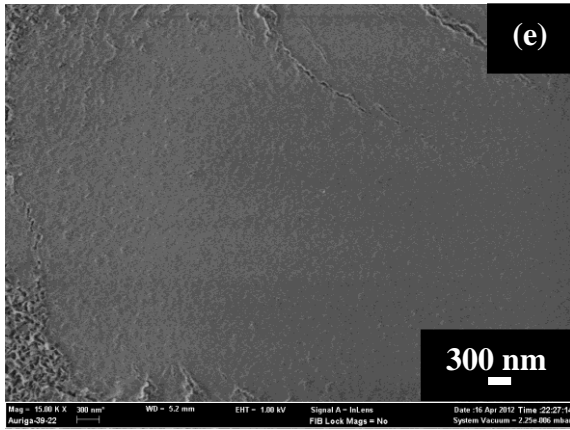
0 day

1 day

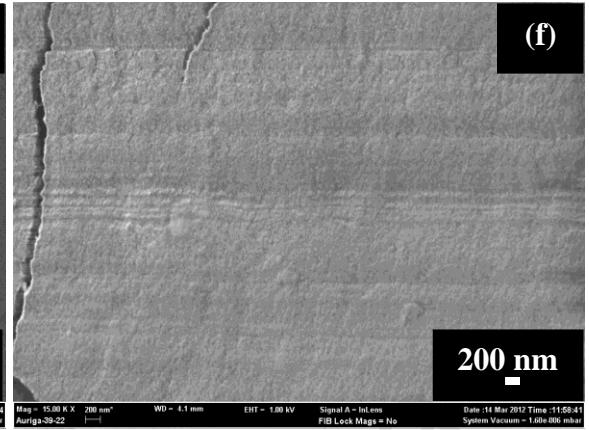


3 days

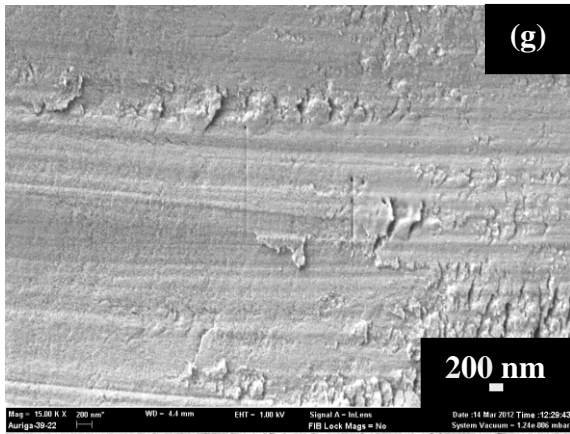
7 days



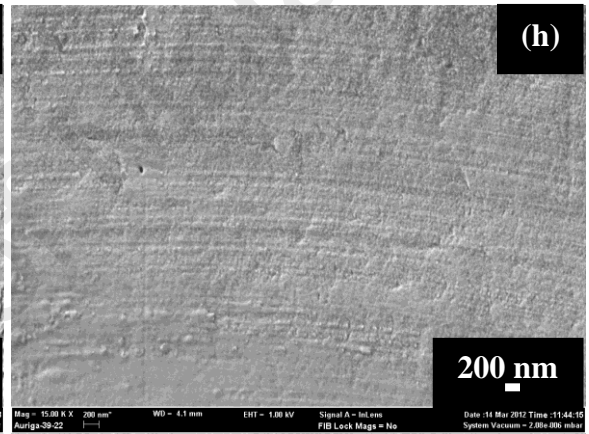
14 days



21 days



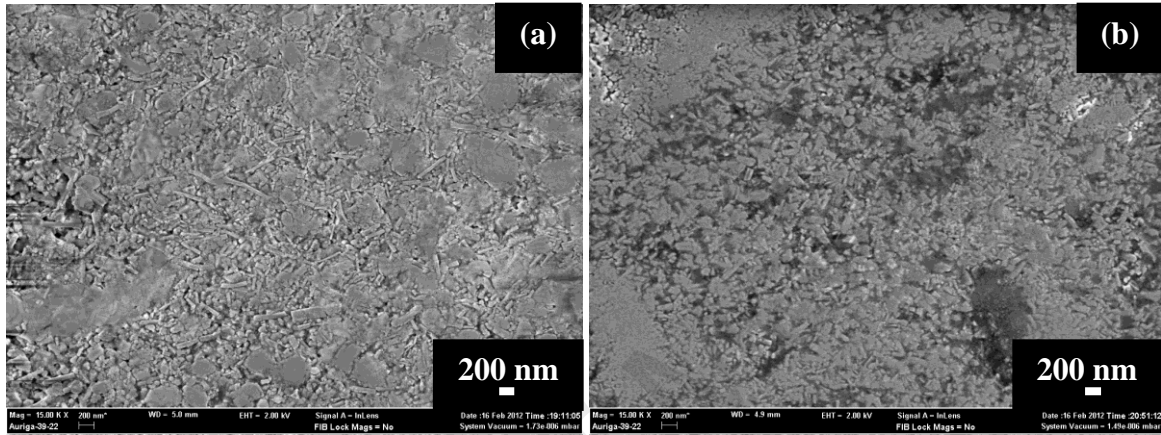
28 days



35 days

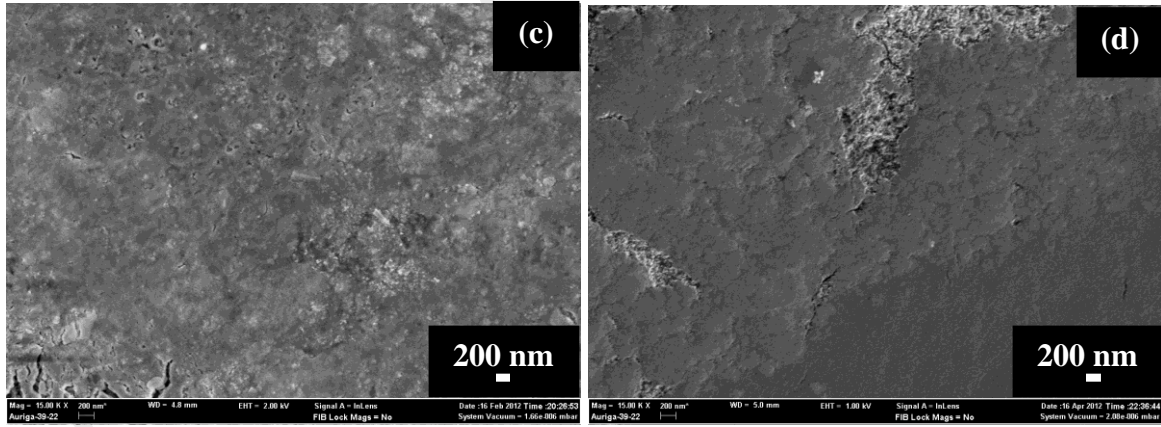
Figure 4.10: FESEM images of the end of scratch track edge scratched at 100mN load (15 k magnification)

At the scratch load of 300 mN, the surface is almost totally flattened after 7 days of immersion in SBF (Figure 4.11(d)) and grooves starts to appear after 28 days (Figure 4.11(g)).



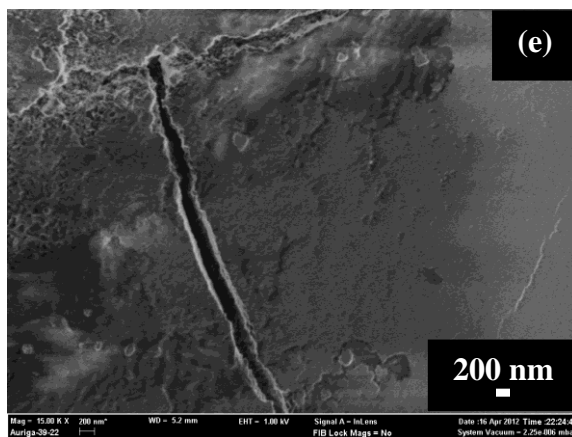
0 day

1 day

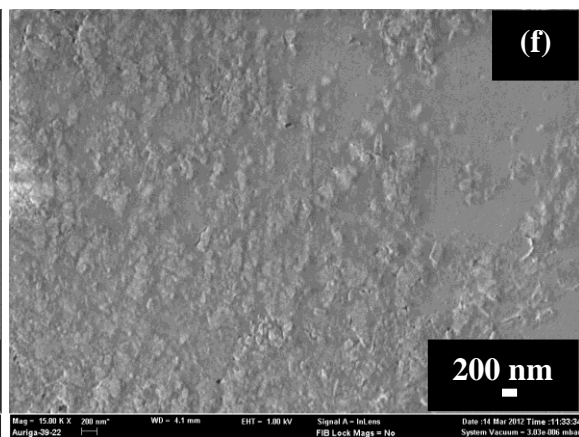


3 days

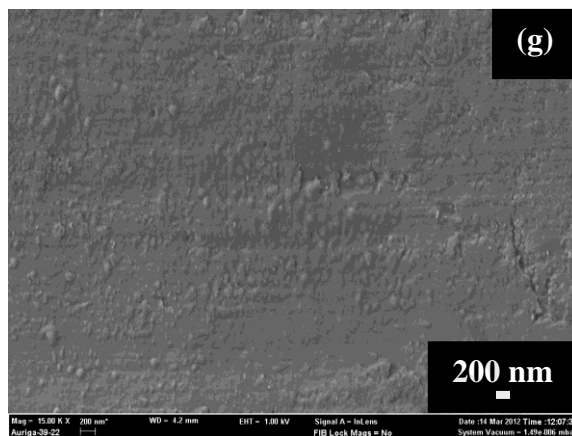
7days



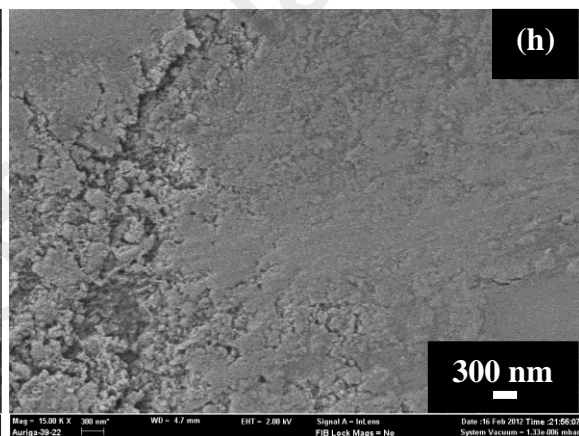
14 days



21 days



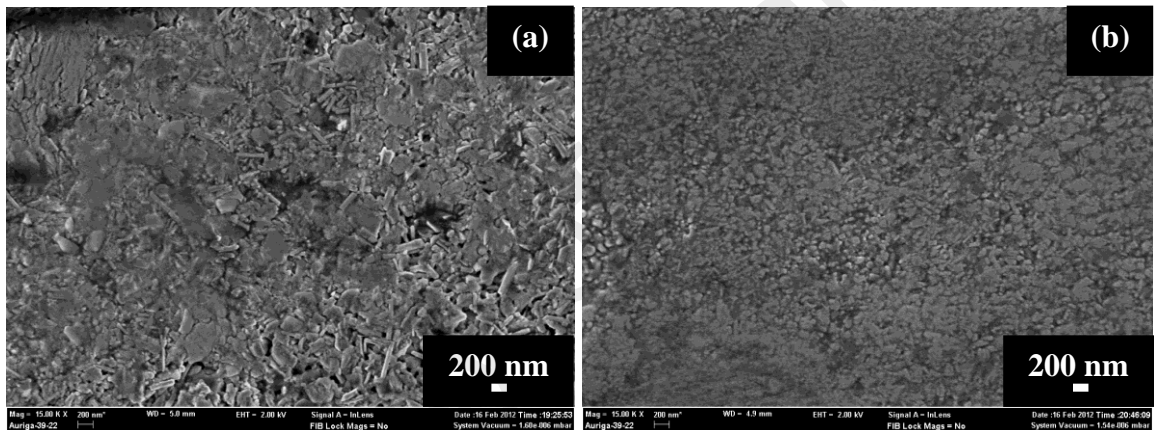
28 days



35 days

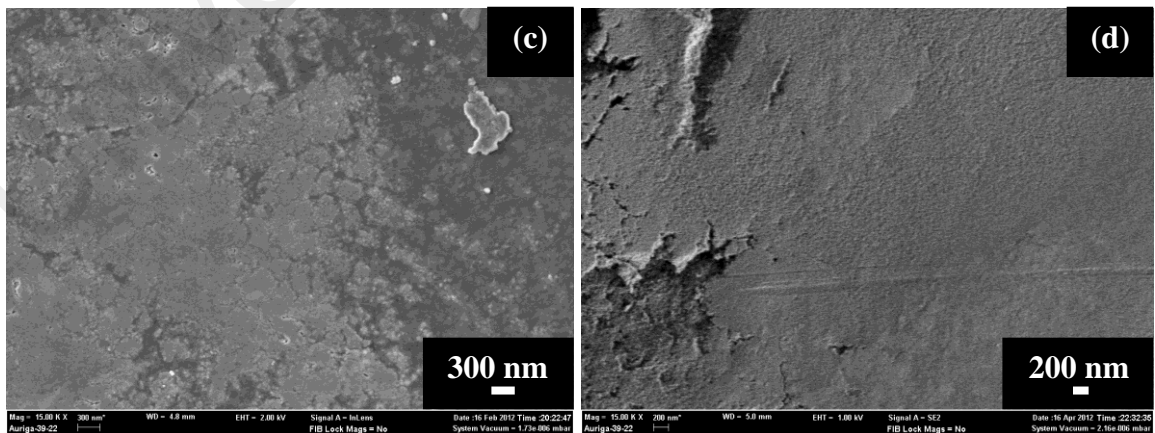
Figure 4.11: FESEM images of the end of scratch track edge scratched at 300mN load (15 k magnification)

As discussed earlier, when the newly grown HA layer becomes thicker upon immersion in SBF, the layer surface becomes softer than the original HA embedded layer. That is why, for a higher scratch load (500 mN), the flattened surface is observed after 3 days of immersion in SBF (Figure 4.12(c)). Scratch grooves are more noticeable here than in the lower load condition as discussed before. However, even at the maximum scratch load of 500 mN, the surface of the substrate is still not revealed in any of the determined immersion condition.



0 day

1 day



3 days

7 days

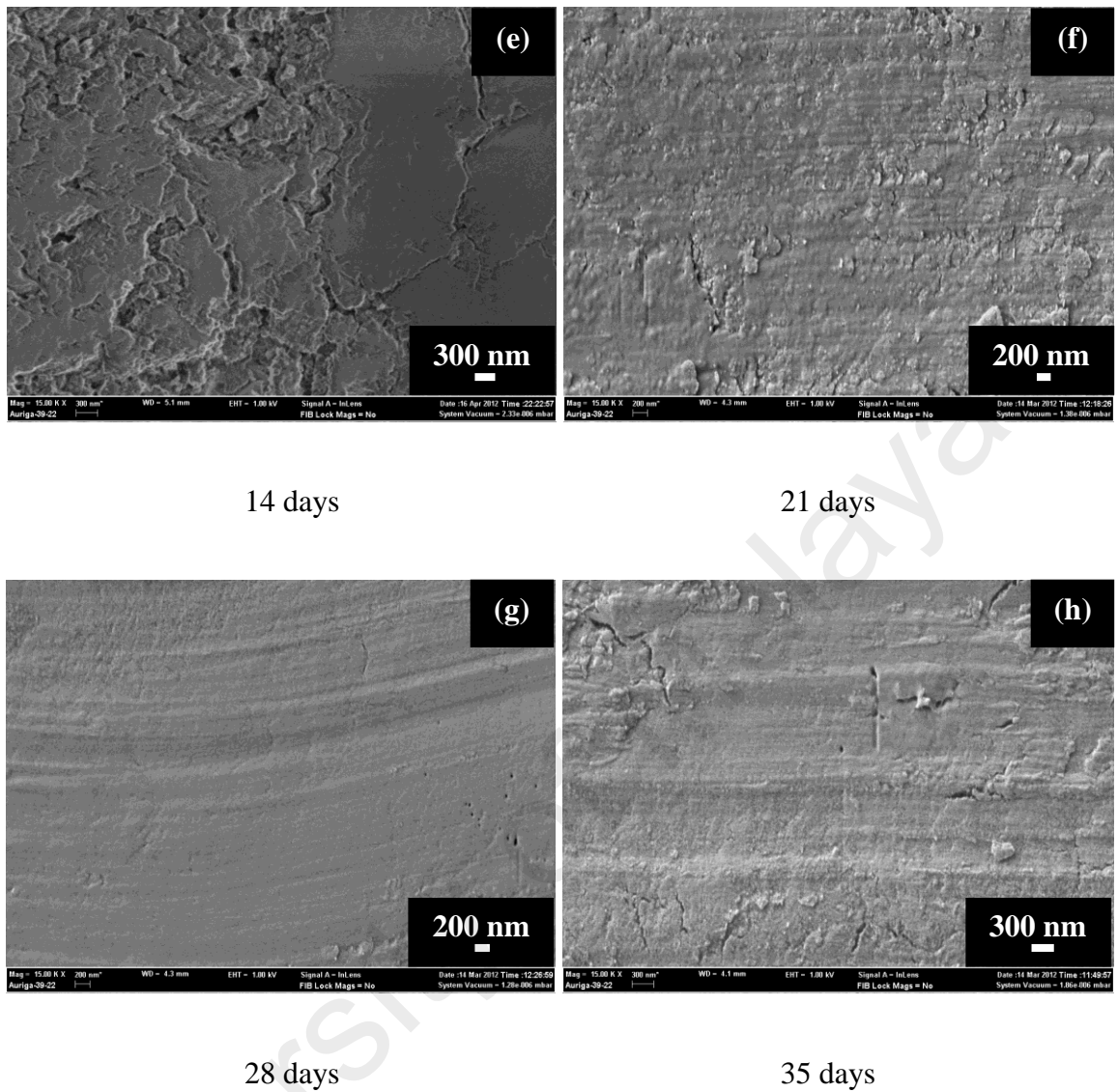


Figure 4.12: FESEM images of the end of scratch track edge scratched at 500mN load (15 k magnification)

Figure 4.13(a-b) indicates the EDX analysis of two different regions on the scratch track edge of a sample which has been submitted to the longest immersion duration of 35 days in SBF and the highest scratch load of 500 mN. It is observed that there are some areas (such as the one labeled by + sign in Figure 4.13(a)) which are not peeled off and show higher Ca and P contents (Figure 4.13(a) and Table 4.2). In some areas (such as the

one labeled by + sign in Figure 4.13(b)), the HA embedded layer peels off, however without reaching the substrate. On the peeled-off region, Ca and P peaks are able to be detected (Figure 4.13(b) and Table 4.3) and this demonstrates that the HA embedded layer is still strongly intact to the substrate. In comparison with the EDX spectrum of the original HA embedded layer (Figure 4.2), since higher Ca and P peaks are observed here it can be suggested that the HA precipitates that have formed during the immersion process have penetrated deep into the HA embedded layer through the pores.

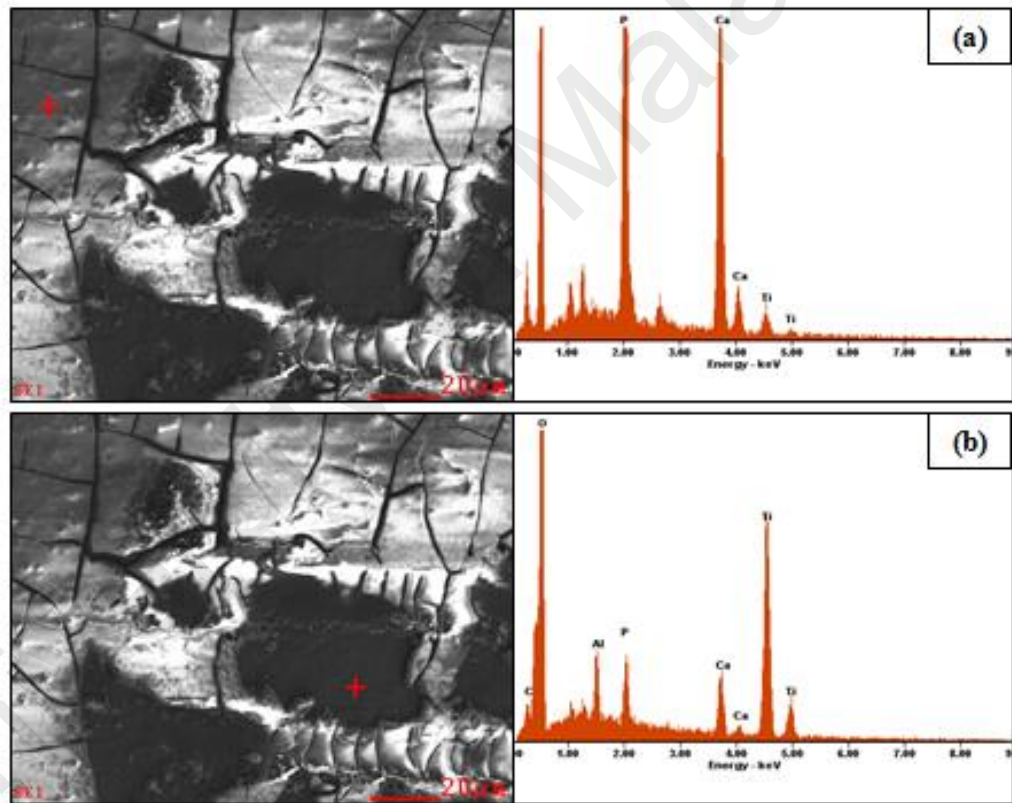


Figure 4.13: EDX spectra of the end of scratch track edge, focusing on the (a) unpeeled-off and (b) peeled-off area of the HA layer of a sample immersed for 35 days in SBF

Table 4.2: Elemental percentage of EDX spectrum (Figure 4.13(a)) of the end of scratch track edge, focusing on the unpeeled-off area of the HA layer of a sample immersed for 35 days in SBF

Element	Wt %	At %
PK	32.75	39.12
CaK	59.36	54.79
TiK	7.88	6.09

Table 4.3: Elemental percentage of EDX spectrum (Figure 4.13(b)) of the end of scratch track edge, focusing on the peeled-off area of the HA layer of a sample immersed for 35 days in SBF

Element	Wt %	At %
AlK	4.06	6.66
PK	5.43	7.77
CaK	10.64	11.75
TiK	79.87	73.82

In some areas, peeling off the HA embedded layer is observed. However, EDX analysis on the area shows that Ca and P peaks are able to be detected and this

demonstrates that the peeling off does not reach until the substrate's surface and the HA embedded layer strongly intact to the substrate even after immersion in SBF for a long period of time. The results also indicate the potential for application of the method for the formation of prosthetic devices

University of Malaya

CHAPTER 5

CONCLUSIONS AND RECOMMENDATIONS

5.1 Conclusions

In this research, a new method is applied for the embedment process of HA powder on the Ti-6Al-4V substrate. The properties of the HA embedded layer are evaluated in terms of its bioactivity and mechanical strength. The following conclusion can be drawn from the experimental results obtained:

- (a) Through superplastic embedment, a HA embedded layer having a thickness of 249 nm and hardness of 660 HV is successfully produced.
- (b) The HA embedded nanolayer contains a sufficient amount of HA elements which provide a bioactive surface on the layer suitable for bone ongrowth.
- (c) The produced surface morphology of the HA embedded layer with the significant amount of pores provide the suitable environment to support tissue adhesion and growth.
- (d) The HA embedded nanolayer is capable of withstanding longer immersion in SBF and a higher scratch load which indicates its excellent mechanical properties.

5.2 Recommendations

The recommendations for further research are as follows:

- (a) It is recommended to carry out the superplastic embedment under vacuum environment for better results due to the high reactivity of Ti-6Al-4V to nature.
- (b) Longer immersion in SBF is recommended for more convincing results.
- (c) Since the produced HA embedded layer is successfully tested in vitro, further investigation should be carried out in vivo.

University of Malaysia

REFERENCES

- Ahmed, H.S.T., & Jankowski, A.F. (2011). Strain rate sensitivity of hydroxyapatite coatings. *Thin Solid Films*, 520, 1516-1519.
- Azevedo, C.R.F., & Santos, A.P.D. (2003). Environmental effects during fatigue testing: fractographic observation of commercially pure titanium plate for cranio-facial fixation. *Engineering Failure Analysis*, 10, 431-442.
- Bai, B.Z., Sun, X.J., Gu, J.L., & Yang, L.Y. (2001) Superplastic behavior of a Ti-alloy with sub-micro structure. *Materials Science Forum*, 357-359, 105-110.
- Bal Seal Engineering Inc. (2009). Titanium Grade 5 (Ti-6Al-4V). Retrieved December 16, 2011 from <http://www.balseal.com/sites/default/files/Titanium%20Grade%205%20%28Ti-6Al-4V%29.pdf>
- Barbieri, F.C., Otani, C., Lepienski, C.M., Urruchi, W.I., & Maciel, H.s. (2002). Nanoindentation study of Ti6Al4V alloy nitride by low intensity plasma jet process. *Vacuum: Surface Engineering, Surface Instrumentation and Vacuum Technology*, 67, 457-461.
- Brooks, C.R., & Choudhury, A. (1993). *Metallurgical Failure Analysis*, McGraw-Hill, Texas.
- Caceres, D., Ocal, C., Jimenez J.A., Gutierrez, A., & Lopez, M.F. (2008). Nanomechanical properties of surface-modified titanium alloys for biomedical applications. *Acta Biomaterialia*, 4, 1545-1552.
- Callister, W.D. (2007). *Materials Science and Engineering: Introduction*. John Wiley & Sons, United States.
- Chai, C.S., & Ben-Nissan, B. (1999). Bioactive nanocrystalline sol-gel hydroxyapatite coatings. *Journal of Materials Science: Materials in Medicine*, 10, 465-469.
- Chandra, N. (2002). Constitutive behavior of superplastic materials. *International Journal of Non-Linear Mechanics*, 37, 461-484.
- Cleries, L., Martinez, E., Fernandez-Pradas, J.M., Sardin, G., Esteve, J., & Morenza, J.L. (2000). Mechanical properties of calcium phosphate coatings deposited by laser ablation. *Biomaterials*, 21, 967-971.

- Collier, J.P., Surprenant, V.A., Mayor, M.B., Wrona, M., Jensen, R.E., & Surprenant, H.P. (1993). Loss of hydroxyapatite coating on retrieved, total hip components. *Journal of Arthroplasty*, 8(4), 389-393.
- Combres, Y., & Blandin, J.J. (1995). Comparison of the β -CEZ and Ti-64 superplastic properties. *Proceedings of the Conference "Titanium '95: Science and Technology"*, Birmingham, 864-871.
- Conforto, E., Aronsson, B.-O., Salito, A., Crestou, C., & Caillard, D. (2004). Rough surfaces of titanium and titanium alloys for implants and prostheses. *Materials Science and Engineering C*, 24, 611-618.
- Cook, S.D., Thomas, K.A., & Kay, J.F. (1991). Experimental coating defects in hydroxyapatite-coated implants. *Clinical Orthopedics and Related Research*, 265, 280-290.
- Czarnowska, E., Wierzchon, T., Maranda-Niedbala, A. (1999). Properties of the surface layers on titanium alloy and their biocompatibility in in vitro tests. *Journal of Materials Processing Technology*, 92-93, 190-194.
- Das, K., Balla, V.K., Bandyopadhyay, A., & Bose, S. (2008) Surface modification of laser-processed porous titanium for load-bearing implants. *Scripta Materialia*, 59, 822-825.
- De Jonge, L.T., Leeuwenburgh, S.C.G., Van Den Beucken, J.J.J.P., Te Riet, J., Daamen, W.F., Joop Wolke, J.G.C., Scharnweber, D., & Jansen, J.A. (2010). The osteogenic effect of electrosprayed nanoscale collagen/calcium phosphate coatings on titanium. *Biomaterials*, 31, 2461-2469.
- Demaïd, A. (1992). A history of superplastic metals [in:] de Wit, J.H.W., Demaid, A., & Onillon, M. *Case studies in manufacturing with advanced materials, North-Holland, Amsterdam*, 1, 35-71.
- Dieter, G.E. (1986). *Mechanical Metallurgy*, Third Edition, McGraw-Hill Book Co.
- Ding, S.J. (2003). Properties and immersion behavior of magnetron-sputtered multi-layered hydroxyapatite/ titanium composite coatings. *Biomaterials*, 24, 4233-4238.
- Ding, S.J., Su, Y.M., Ju, C.P., & Lin, J.H.C. (2001). Structure and immersion behavior of plasma sprayed apatite-matrix coatings. *Biomaterials*, 22, 833-845.
- Dom, A.H.M., Jauhari, I., Parast, S.Y., & Khalid, H.M. (2010). Embedment of HA/Ti composite on superplastic titanium alloy (Ti-6Al-4V). *Materials Science and Engineering A*, 527, 5831-5836.

Elias, K.L., Daehn, G.S., Brantley, W.A., & McGlumphy, E.A. (2007). An initial study of diffusion bonds between superplastic Ti-6Al-4V for implant dentistry applications. *Journal of Prosthetic Dentistry*, 97(6), 357-65.

Fonseca, J.C., Henriques, G.E.P., Sobrinho L.C., & Goes, M.F.D. (2003). Stress-relieving and porcelain firing cycle influence on marginal fit of commercially pure titanium and titanium–aluminum–vanadium copings. *Dental Materials*, 19, 686-691.

Froes, F.H., & Bomberger, H.B., (1985). The beta titanium alloys. *Journal of Metals*, 37, 28-37.

Frommeyer, G., & Rommerskirchen, M. (1995). Structural super-plasticity in a micro duplex γ - TiAl / α_2 - Ti₃Al alloy. Proceedings of the Conference “Titanium ’95: Science and Technology”, Birmingham, 239-247.

Goldstein, J.I., Newbury, D.E., Echlin, P., Joy, D.C., Lyman, C.E., Lifshin, E., Sawyer, L., & Michael, J.R. (2003). Scanning Electron Microscopy and X-Ray Microanalysis. Springer, New York.

Gordon England. (2008). Microhardness Test. In Surface Engineering Forum. Retrived October 15, 2011, from <http://www.gordonengland.co.uk/hardness/microhardness.htm>

Grabski, M. (1973). Fine-structure superplasticity in metals. *Silesian Press, Katowice (in Polish)*.

Gu, Y.W., Khor, K.A., & Cheang, P. (2003). In vitro studies of plasma-sprayed hydroxyapatite/Ti-6Al-4V composite coatings in simulated body fluid (SBF). *Biomaterials*, 24, 1603-1611.

Hamdi, M., & Ktessabi, A.M. (2001). Electron beam deposition of thin bioceramic film for biomedical implants. *Thin Solid Films*, 398, 386-390.

Hamilton, C. H., Ash, B. A., Sherwood, D., & Heikkinen, H. C. (1988). Superplasticity in Aerospace. *H.C. Heikkinen, T.R. McNelley (Eds.), TMS Publishers, Pennsylvania*, 29-50.

Hench, L.L. (1998). Bioceramics. *Journal of the American Ceramic Society*, 81, 1705-1728.

Higashi, K., & Mabuchi, M. (1997) *Materials Science Forum*, 32, 243-245.

Hiraga, T., Miyazaki, T., Tasaka, M., & Yoshida, H. (2010). Mantle superplasticity and its self-made demise. *Nature*, 468(7327), 1091-1094, doi: 10.1038/nature09685

Hofmann, H., Frommeyer, G., & Herzog, W. (1995). Dislocation creep controlled superplasticity at high strain rates in the ultrafine grained quasi-eutectoid Ti-10Co-4Al alloy. *Proceedings of the Conference "Titanium '95: Science and Technology"*, Birmingham, 833-840.

Hori, S., Tokzane, M., & Furushiro N. (Eds.) (1991). Superplasticity in Advanced Materials (ICSAM-91), Japan Society for Research on Superplasticity, Osaka, Japan, 1991.

Hsiao, I. C., & Huang, J. C. (2002) Deformation Mechanisms during Low- and High-Temperature Superplasticity in 5083 Al-Mg Alloy. *Metallurgical And Materials Transactions A*, 33A, 1373-1384.

Hsieh, M.F., Perng, L.H., & Chin, T.S. (2002). Hydroxyapatite coating on Ti6Al4V alloy using a sol-gel derived precursor. *Materials Chemistry and Physics*, 74, 245-250.

Imayev, V.M., Salishchev, G.A., Shagiev, M.R., Kuznetsov, A.V., Imayev, R.M., Senkov, O.N., & Froes, F.H. (1999). Low-temperature superplasticity of submicrocrystalline Ti-48Al-2Nb-2Cr alloy produced by multiple forging. *Scripta Materialia*, 40(2),183-190.

Inagaki, H. (1995). Enhanced superplasticity in high strength Ti alloys. *Zeitschrift fur Metallkunde*, 86(9), 643-650.

Inagaki, H. (1996). Mechanism of enhanced superplasticity in thermomechanically processed Ti-6Al-4V. *Zeitschrift fur Metallkunde*, 87(3), 179-186.

Jansen, J., Waerden, J.V., Wolke, J., & De Groot, K. (1991). Histologic evaluation of the osseous adaptation to titanium and hydroxyapatite-coated titanium implants. *Journal of Biomedical Materials Research*, 25, 973-989.

Javed, F., & Romanos, G.E. (2010). The role of primary stability for successful immediate loading of dental implants-A literature review. *Journal of Dentistry*, 38, 612-620.

Joshi, V.A. (2006). Titanium Alloys, An Atlas of Structures and Fracture Features. *Taylor & Francis*.

Kaibyshev, O.A. (2002). Fundamental aspects of superplastic deformation. *Materials Science and Engineering A*, 324, 96-102.

Karasevskaya, O.P., Ivasishin, O.M., Semiatin, S.L., & Matviychuk, Y.V., (2003). Deformation behavior of beta-titanium alloys. *Materials Science and Engineering A*, 354, 121-132.

Khalid, H.M., Jauhari, I., Jamlus, S.A., & Dom, A.H.M. (2012). High temperature deformation of Ti alloy superplastically embedded with HA. *Material Science and Engineering A*, 524, 37-42.

Kim, J.H., Park, C.G., Ha, T.K., & Chang, Y.W. (1999). Microscopic observation of superplastic deformation in a 2-phase Ti3Al-Nb alloy. *Materials Science Engineering A*, 269, 197-204.

Kobayashi, M., Ochiai, S., Funami, K., Ouchi, C., & Suzuki, S. (1994). Superplasticity of fine TiC and TiN dispersed Ti-6Al-4V alloy composites. *Materials Science Forum*, 170-172, 549-554.

Kokubo, T. (1991). Bioactive glass ceramics: properties and applications. *Biomaterials*, 12, 155-163.

Kokubo, T., Kushitani, H., Kitsugi, S., & Yamamuro, T. J. (1990). Solutions able to reproduce in vivo surface-structure changes in bioactive glass-ceramic A-W. *Journal of Biomedical Materials Research*, 24, 721-734.

Kokubo, T., & Takadama, H. (2006). How useful is SBF in predicting in vivo bone bioactivity? *Biomaterials*, 27, 2907-2915.

Ktessabi, A.M., & Hamdi, M. (2002). Characterization of calcium phosphate bioceramic films using ion beam analysis techniques. *Surface and Coatings Technology*, 153(1), 10-15.

Kulikowski, Z., Wisbey, A., & Ward-Close, C.M. (1995). Superplastic deformation in the biomedical titanium alloy Ti-6Al-7Nb (IMI 376). *Proceedings of the Conference "Titanium '95: Science and Technology"*, Birmingham, 909-916.

Kweh, S.W.K., Khor, K.A., & Cheang, P. (2000). Plasma-sprayed hydroxyapatite (HA) coatings with flame-spheroidized feedstock: microstructure and mechanical properties. *Biomaterials*, 21(12), 1223-1234.

Langdon, T. G., (1994). An evaluation of the strain contributed by grain-boundary sliding in superplasticity. *Material Science and Engineering A*, 174, 225-230.

Langdon, T. G., (2009). Seventy-five years of superplasticity: historic developments and new opportunities. *Journal of Materials Science*, 44, 5998–6010.

Latka, L., Pawlowski, L., Chicot, D., Pierlot, C., & Petit, F. (2010). Mechanical properties of suspension plasma sprayed hydroxyapatite coatings submitted to simulated body fluid. *Surface and Coatings Technology*, 205, 954-960.

Leyens C., & Peters, M. (2003). Titanium and Titanium Alloys. *Fundamentals and Applications*. Cologne.

Liu, D.M., Yang, Q.Z., Troczynski, T., & Tseng, W.J.J. (2002). Structural evolution of sol-gel derived hydroxyapatite. *Biomaterials*, 23(7), 1679-1687.

Liu, F., Wang, F., Shimizu, T., Igarashi, K., Zhao, L. (2005) Formation of hydroxyapatite on Ti-6Al-4V alloy by microarc oxidation and hydrothermal treatment. *Surface and Coatings Technology*, 199, 220-224.

Liu, F. C., Xiao, B. L., Wang, K., & M, Z. Y. (2010) Investigation of superplasticity in friction stir processed 2219Al alloy. *Materials Science and Engineering A* 527, 4191-4196

Liu, X., Chu, P.K., & Ding, C.H. (2004). Surface modification of titanium, titanium alloys, and related materials for biomedical applications. *Materials Science and Engineering: R: Reports*, 47, 49-121.

Long, M.J., & Rack, H.J. (1998). Titanium alloys in total joint replacement-a materials science perspective. *Biomaterials*, 19, 1621-1639.

Lynn, A.K., & DuQuesney, D.L. (2002). Hydroxyapatite-coated Ti-6Al-4V Part 1: the effect of coating thickness on mechanical fatigue behavior. *Biomaterials*, 23(9), 1937-1946.

MacDonald, D.E., Betts, F., Stranick, M., Doty, S., & Boskey, A.L. (2001). Physicochemical study of plasma-sprayed hydroxyapatite-coated implants in humans. *Journal of Biomedical Materials Research*, 54(4), 480-490.

Mallikarjun, K., Suwas, S., & Bhargava, S., (2003). Effect of prior β processing on superplasticity of ($\alpha+\beta$) thermo-mechanically treated Ti-632Si alloy. *Materials Technology*, 134, 35-44.

Martin, R., & Evans, D. (2000). Reducing costs in aircraft: The metals affordability initiative consortium. *Journal of The Minerals, Metals and Materials Society*, 52(3), 24-28.

Materials Evaluation and Engineering Inc. (2009). Energy Dispersive X-Ray Spectroscopy. Retrieved October 2, 2012 from <http://mee-inc.com/eds.html>

Meng, X., Kwon, T.Y., & Kim, K.H. (2008). Hydroxyapatite coating by electrophoretic deposition at dynamic voltage. *Dental Materials*, 27(5), 666-671.

Mukherjee, A.K. (2002). An examination of the constitutive equation for elevated temperature plasticity. *Materials Science Engineering A*, 322, 1-22.

Mittal, K.L. (1995). Adhesion Measurement of Films and Coatings, *VSP BV, Utrecht*.

Nakahigashi, J., & Yoshimura, H. (2002). Ultra-fine grain refinement and tensile properties of titanium alloys obtained through protium treatment. *Journal of Alloys and Compounds*, 330–332, 384–388.

Narayanan, R., Dutta, S., & Seshadri, S.K. (2006). Hydroxyapatite coatings on Ti-6Al-4V from seashell. *Surface and Coatings Technology*, 200, 4720 – 4730.

Narayan, R. A., Jayaprakasan, K., Balachander. V. K., & Bhattacharjee, J. B. (2010). Automation of superplastic formation using virtual instrumentation, *GESJ: Computer Science and Telecommunications*, 3, 26.

Nie, X., Leyland, A., & Matthews, A. (2000). Deposition of layered bioceramic hydroxyapatite/TiO₂ coatings on titanium alloys using a hybrid technique of micro-arc oxidation and electrophoresis. *Surface and Coatings Technology*, 125(1-3), 407-414.

Nieh, T.G., Wadsworth, J., & Sherby, O.D. (1997). Superplasticity in Metals and Ceramics. *Cambridge University Press, Cambridge*.

Niespodziana, K., Jurczyk, K., & Jurczyk, M. (2006). The manufacturing of titanium-hydroxyapatite nanocomposites for bone implant applications. *Nanopages*, 1, 219-229.

Nonami, T., Kamiya, A., Naganuma, K., & Kameyana, T. (1998). Implantation of hydroxyapatite granules into superplastic titanium alloy for biomaterials. *Materials Science and Engineering C*, 6, 281-284.

Ogawa, A., Iizumi, H., & Minakawa, K. (1995). Superplasticity and post-SPF properties of SP-700. *Proceedings of the Conference "Titanium '95: Science and Technology"*, Birmingham, 588-595.

Parast, S.Y., Jauhari, I., & Zaeem, M.A. (2011). Implantation of HA into superplastic Ti-6Al-4V: kinetics and mechanical behavior of implanted layer. *Metallurgical and Materials Transactions A- Physical Metallurgy and Materials Science*, 42, 219-226.

Polmear, I.J. (1981). *Light alloys from traditional alloys to nanocrystals*, Melbourne.

Pu, H. P., Liu, F. C., & Huang, J. C. (1995). Characterization and Analysis of Low-Temperature Superplasticity in 8090 Al-Li Alloys. *Metallurgical and Materials Transaction A*, 26A, 1153-1166.

Radin, S.R., and Ducheyne, P. (1992). Plasma spraying induced changes of calcium-phosphate ceramic characteristics and the effect on in vitro stability. *Journal of Materials Science: Materials in Medicine*, 3 (1), 33-42.

Rickerby, D.S. (1988). A review of the methods for the measurement of coating-substrate adhesion. *Surface and Coatings Technology*, 36, 541-557.

Saber-Samandari S., Berndt C.C., & Gross K.A. (2011). Selection of the implant and coating materials for optimized performance by means of nano-indentation. *Acta Biomaterialia*, 7(2), 874-881.

Salishchev, G.A., Murzinova, M.A., Zherebtsov, S.V., Afonichev, D.D., S.P. Malysheva, S.P. (2001). Influence of reversible hydrogen alloying on formation of SMC structure and superplasticity of titanium alloys. *Materials Science Forum*, 357-359, 315-320.

Sherby, O. D., & Wadsworth, J. (1984). *Deformation, Processing and Structure*, G. Krauss, ed., ASM, Metals Park, OH, 355-365.

Shi, D. (2004) *Biomaterials and Tissue Engineering*. Springer, Berlin Heidelberg, New York.

Sieniawski, J., & Motyka, M. (2007). Superplastic in titanium alloys. *Materials and Manufacturing Engineering*, 24(1), 123-130.

Smith, W.F. (1993). *Structure and Properties of Engineering Alloy*, 2nd edition, McGraw-Hill.

Simmons, C.A., Valiquette, N., & Pilliar, R.M. (1999). Osseointegration of sintered porous-surfaced and plasma spray-coated implants: An animal model study of early postimplantation healing response and mechanical stability. *Journal of Biomedical Materials Research*, 47(2), 127-138.

Suchanek, W., & Yoshimura, M. (1998). Processing and properties of hydroxyapatite – based biomaterials for use as hard tissue replacement implants. *Journal of Materials Research*, 13, 94-117.

Tattner, B.D., Hoffman, A.S., Schoen, F.J., & Lemons, J.E. (eds). (2004). *Biomaterials Science*, 2nd ed. Elsevier, Academic Press, San Diego, USA, 162-166.

Tisler, R.J., Lederich, R.J. (1995). Advanced superplastic titanium alloys. *Proceedings of the Conference "Titanium '95: Science and Technology"*, Birmingham, 596-603.

Toque, J.A., Herliansyah, M.K., Hamdi, M., Ide-Ektessabi, A., Sopyan, I. (2010). Adhesion failure behavior of sputtered calcium phosphate thin film coatings evaluated using microscratch testing. *Journal of Mechanical Behaviour of Biomedical Materials*, 3, 324-330.

Valli, J. (1986). A review of adhesion test methods for thin hard coatings. *Journal of Vacuum Science and Technology A*, 4, 3007-3014.

Vetrano, J.S. (2001). Superplasticity: mechanisms and applications, *JOM Journal of The Minerals, Metals & Materials Society*, 53, 22.

Wang, C.K., Chern, L.J.H., Ju, C.P., Ong, H.C., & Chang, R.P.H. (1997). Structural characterization of pulsed laser deposited hydroxyapatite film on titanium substrate. *Biomaterials*, 18, 1331-1338.

Wang, K. (1996). The use of titanium for medical applications in the USA. *Materials Science and Engineering A*, 213, 134-137.

Wei, M., Ruys, A.J., Milthorpe, B.K., & Sorrell, C.C. (1999). Solution ripening of hydroxyapatite nanoparticles: effects on electrophoretic deposition. *Journal of Biomedical Resolution*, 45, 11-19.

Xinghao, D., Baolin, J. C., & Huang, J. C. (2007). Superplastic deformation behavior of a spray-deposited eutectic NiAl/Cr(Mo) alloy doped with Dy. *International Journal of Materials and Resolution*, 98, 2.

Xuhui, Z., Lingfang, Y., Yu, Z., & Jinping, X. (2009). Hydroxyapatite coatings on titanium prepared by electrodeposition in a modified simulated body fluid. *Chinese Journal of Chemical Engineering*, 17(3), 667-671.

Yao, S.H., Kao, W.H., Su, Y.L., & Liu, T.H. (2004). On the tribology and micro-drilling performance of TiN/AlN nanolayer coatings. *Materials Science and Engineering A*, 386, 149-155.

Yildirim, O.S., Aksakal, B., Celik, H., Vangolu, Y., & Okur, A. (2005). An investigation of the effects of hydroxyapatite coatings on the fixation strength of cortical screws. *Medical Engineering and Physics*, 27, 221-228.

Zhang, S., Xianting, Z., Yongsheng, W., Kui, C., & Wenjian, W. (2006). Adhesion strength of sol-gel derived fluoridated hydroxyapatite coatings. *Surface and Coatings Technology*, 200, 6350-6354.